# A large deformation viscoelastic model for double-network hydrogels

Yunwei Mao, Shaoting Lin, Xuanhe Zhao, Lallit Anand*

*Department of Mechanical Engineering, Massachusetts Institute of Technology, Cambridge, MA 02139, USA*

A B S T R A C T

We present a large deformation viscoelasticity model for recently synthesized double network hydrogels which consist of a covalently-crosslinked polyacrylamide network with long chains, and an ionically-crosslinked alginate network with short chains. Such double-network gels are highly stretchable and at the same time tough, because when stretched the crosslinks in the ionically-crosslinked alginate network rupture which results in distributed internal micro-damage which dissipates a substantial amount of energy, while the configurational entropy of the covalently-crosslinked polyacrylamide network allows the gel to return to its original configuration after deformation. In addition to the large hysteresis during loading and unloading, these double network hydrogels also exhibit a substantial rate-sensitive response during loading, but exhibit almost no rate-sensitivity during unloading. These features of large hysteresis and asymmetric rate-sensitivity are quite different from the response of conventional hydrogels. We limit our attention to modeling the complex viscoelastic response of such hydrogels under isothermal conditions. Our model is restricted in the sense that we have limited our attention to conditions under which one might neglect any diffusion of the water in the hydrogel — as might occur when the gel has a uniform initial value of the concentration of water, and the mobility of the water molecules in the gel is low relative to the time scale of the mechanical deformation. We also do not attempt to model the final fracture of such double-network hydrogels.

## 1. Introduction

A gel consists of crosslinked macromolecules and a solvent, and for hydrogels the solvent is water. Conventional hydrogels — which are usually composed of a *single network* of a hydrophilic polymer — have low stiffness, strength, and toughness. Recently, Gong and co-workers (cf., e.g., Gong et al., 2003; Gong, 2010, 2014) have synthesized several *double-network* hydrogels which have high water content, ≈80—90 wt%, and possess mechanical properties which are remarkably superior to those of single network gels.

As is well-known the stiffness of a polymer network increases as its crosslink density increases, but it also becomes more brittle. Double-network (DN) hydrogels consist of two interpenetrating polymer networks with contrasting mechanical properties; cf. Fig. 1(a) for a schematic. The first network is sparsely crosslinked with long chains — so that it is compliant and stretchable, while the second network is densely crosslinked with short chains — making it stiff and brittle. The two polymer networks are interlaced on a molecular scale but not covalently bonded to each other.

• Double-network gels are tough because when stretched the crosslinks in the densely-crosslinked network rupture, resulting in

---
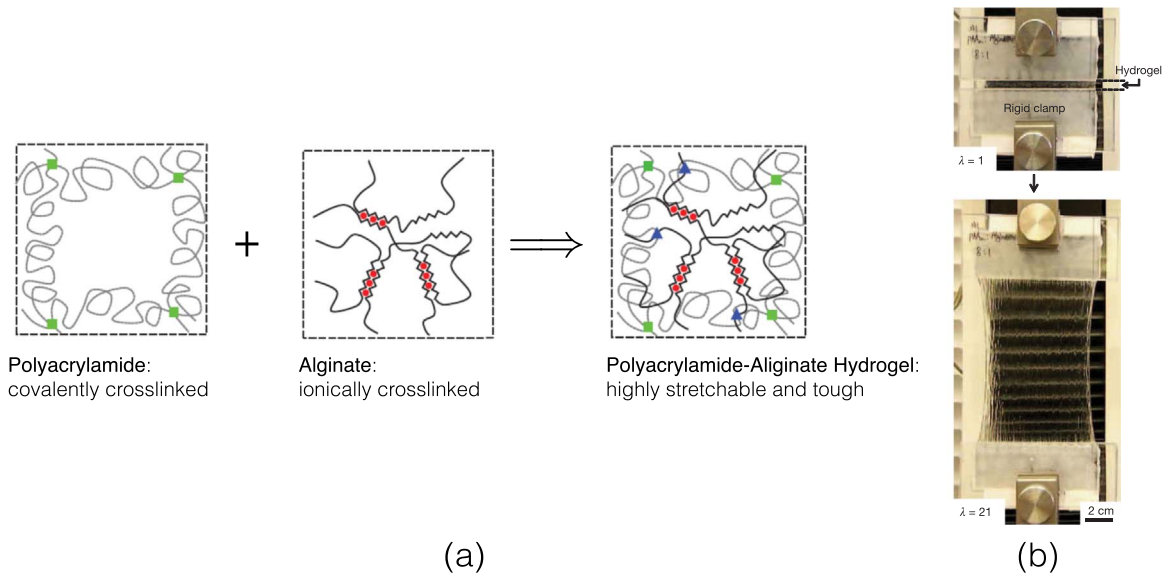
**Fig. 1.** (a) By combining two networks — one with long chains so that it compliant and stretchable, and another with short chains so that it is is stiff and brittle — a *tough double-network gel* may be created. The example shown here is for a double-network PAAm-alginate hydrogel which contains ∼90% water. (b) Photograph of a PAAm-alginate hydrogel being stretched to several times its original length. Adapted from Sun et al. (2012).

distributed internal microdamage which dissipates a substantial amount of energy, while the configurational entropy of the sparsely-crosslinked network allows the gel to return to its original configuration after deformation.

There are several possible processing routes to synthesize double-network-based elastomeric gels in which the two networks have contrasting mechanical properties (cf., e.g., Gong et al., 2003; Sun et al., 2012, 2013; Gong, 2014; Ducort et al., 2014; Zhao, 2014; Zhang et al., 2015). The DN hydrogels synthesized by Sun et al. (2012) and Zhang et al. (2015) consist of a covalently-crosslinked polyacrylamide (PAAm) network with long chains, and an ionically-crosslinked alginate network with short chains. When such a double-network gel is deformed the ionic-crosslinks in the alginate network rupture, resulting in distributed internal microdamage and dissipation due to such microdamage. Such PAAm-alginate gels have been shown to be highly stretchable, cf. Fig. 1(b), and they also possess a high fracture energy up to $\Gamma \approx 9000$ J/m$^2$.

While several interesting characteristics of the mechanical response of double-network hydrogels including Mullins-type effects have been reported in the literature (Wang and Hong, 2012; Zhao, 2012), *to the best of our knowledge there is no published report on a constitutive model for the complex large deformation viscoelastic response of such materials.*[1] The objective of this paper is to present a large deformation viscoelasticity model for the type of DN hydrogels synthesized by Sun et al. (2012) and Zhang et al. (2015). From the outset we restrict the scope of our modeling efforts in the following sense: (i) We limit our attention to conditions under which one might make the approximation that the concentration of water in the gel is spatially and temporally constant, as might occur when the gel has a uniform initial value of the concentration of water and the mobility of the water molecules in the gel is low — relative to the time scale of the mechanical deformation. (ii) We limit our attention to modeling the deformation response of such hydrogels under isothermal conditions. That is, we consider a purely mechanical theory under isothermal conditions, and neglect any diffusion of the water in the hydrogel. We also do not attempt to model the final fracture of such double-network gels.

The plan of this paper is follows. We begin in Section 2 with some experimental results from simple extension experiments on a DN hydrogel of the type studied by Zhang et al. (2015). In Section 3 we summarize a reasonably general continuum theory that we specialize in Section 4 to model the complex viscoelastic response of the DN hydrogel under study. A procedure for estimation of the material parameters in the specialized constitutive equations is discussed in Section 5, where we show that our model can reproduce the major characteristic features of the response of the DN hydrogel, viz., (a) a large Mullins-type effect which manifests itself in hysteresis during loading and unloading; and (b) an asymmetric rate-sensitive response during loading and unloading. These features are quite different from the response of conventional elastomeric gels. In Section 6 we show results from a large deformation double-shear experiment on DN hydrogel and show that our model can also predict the response of the material in double-shear with reasonable accuracy. We close in Section 7 with some final remarks.

---

[1] As pointed out to us by an anonymous Reviewer, there is a very recent paper on this subject by Lu et al. (2017). However, this paper appeared in the literature **after** we had submitted our paper for publication to JMPS.

## 2. Some experimental results from mechanical tests on a DN hydrogel

### 2.1. Sample preparation

Samples of a PAAm-alginate double network (DN) hydrogel, and those of a single-network (SN) PAAm hydrogel were synthesized as follows:

1. **PAAm-alginate double-network hydrogel**:
   - Mixing 5.5 ml of 18.7 wt% acrylamide solution (Sigma, A8887) with 4.2 ml of 4.8 wt% alginate solution (Sigma, A2033).
   - Then: (i) 900 μl 0.2 g/L N′N methylenebisacrylamide (Sigma, 146072); (ii) 108 μl 0.2 M ammonium persulphate (Sigma, 248614); and (iii) 8 μl N,N,N′,N′-tetramethylethylenediamine (Sigma, T7024−50M) were added into the above mixture. Here: (i) N′N methylenebisacrylamide acts as the cross-linker (Sigma, 146072); (ii) ammonium persulphate (Sigma, 248614) as the photoinitiator; and (iii) N,N,N′,N′-tetramethylethylenediamine (Sigma, T7024−50M) acts as the crosslinking accelerator for the PAAm network.
   - After degassing the mixture, 200 μl of 1 M $CaSO_4$ was added into the mixture to crosslink the alginate network.
   - The solution was then poured into a laser-cut plexiglass mold and cured with UV irradiation (254 nm wavlength, at 8.0 mW/$cm^2$) for 60 min.
   - The samples were stored in a humid box for at least 10 h in order to homogenize them before any mechanical testing. All specimens for mechanical testing were cut from the same piece of cured hydrogel in order to obtain consistent data.
2. **PAAm single-network hydrogel**: Additional samples with exactly the same composition as above, but *without* any calcium sulphate were also made. In such samples the alginate system will not be ionically-crosslinked, but the polyacrylamide monomers will be covalently-crosslinked to form a long chain network. We call such samples as "control" single-network (SN) samples.

### 2.2. Experiments

Simple tension experiments on sheet specimens with dimensions shown in Fig. 2a (thickness 1.5 mm) were conducted using a Zwick-Roell mechanical testing machine with a 20N load cell. The axial stretch, $\lambda$, was measured by using a digital-image-correlation (DIC) method, and this DIC-based measurement of the stretch was related to the relative displacement of the gripping lines "O" and "A" (cf. inset in Fig. 2) at the shoulders of the specimens. Fig. 2(b) shows that the DIC-based stretch measurement in the gage section of a specimen and the relative displacement at the grips are linearly related (the dashed line), for stretch rates in the range $\dot\lambda \in [0.4, 35.3]$/min. We used the calibration curve in Fig. 2b to construct the stretch-stress curves for all the data presented in this paper.

Fig. 3a shows a representative engineering (Piola) stress $S$ versus stretch $\lambda$ curve for the SN hydrogel at a stretch rate of 8.8/min during loading. We tested three specimens and the error-bars show the variability of the data for nominally identical specimens. Fig. 3(b) shows representative loading-unloading $S$-$\lambda$ curve for the DN hydrogel at a stretch rate of 8.8/min. Again, we tested three specimens and the error-bars show the variability of the data for nominally identical specimens. The loading-unloading curve for the DN hydrogel shows substantial hysteresis. This large hysteresis loop for the DN gel is a macroscopic manifestation of the breaking of the ionic crosslinks in the alginate network which leads to dissipation; this represents a Mullins-type effect (Mullins, 1969). For comparison the $S$-$\lambda$ loading-unloading curve for the SN hydrogel is also shown in Fig. 3(b), but for the SN hydrogel the difference
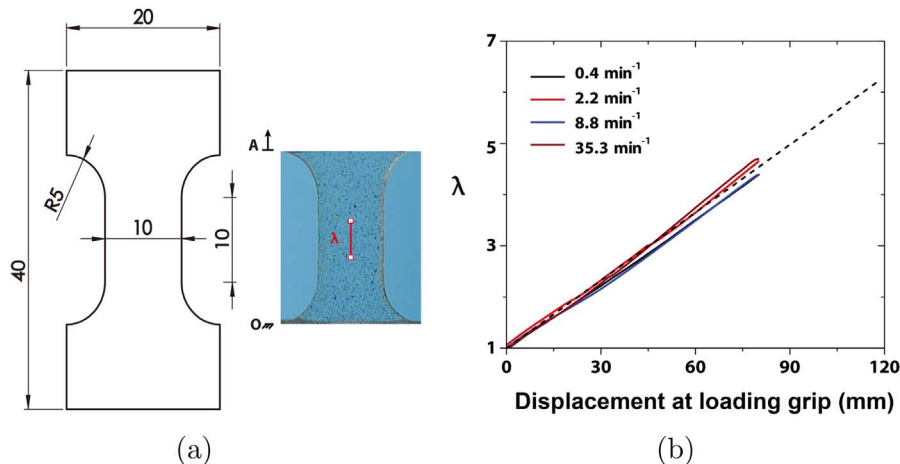


Fig. 2. (a) Dimensions of sheet specimens for simple tension experiments; the specimens were 1.5 mm thick. The inset shows the white gage points used to measure the axial stretch, $\lambda$, by using a digital-image-correlation (DIC) method. The horizontal lines at "O" and "A" in the shoulder region indicate where the specimens were gripped at the shoulders of the dog-bone tension specimens. (b) The DIC-measured stretch at the center of the sample versus the relative displacement of the loading grips at various stretch rates. The dashed line shows the linear relation between stretch and the relative displacement of the loading grips.
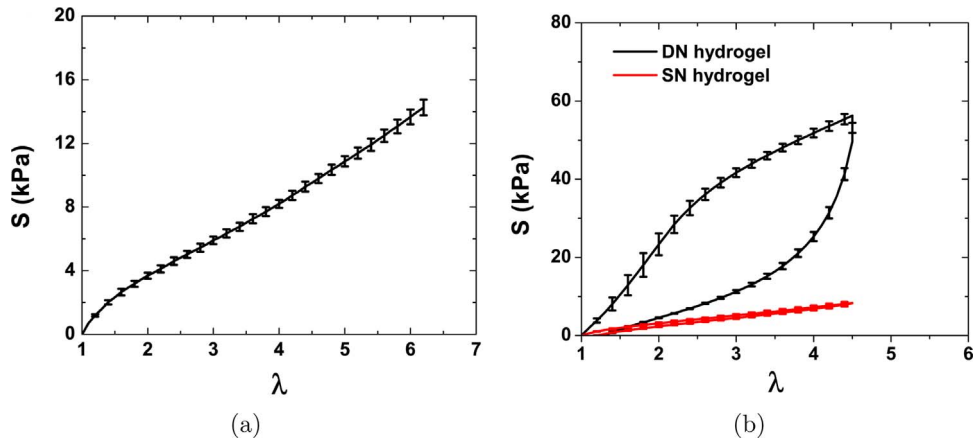
**Fig. 3.** (a) Representative stretch-stress response at a stretch rate of 8.8/min for the SN hydrogel. (b) Representative stretch-stress response at a stretch rate of 8.8/min for DN as well as the SN hydrogels. The error-bars show the variability of the data for nominally identical specimens.

between the loading and the unloading curves at a stretch rate of 8.8/min was less than 0.5 kPa; this small difference is not discernable because of the stress-scale in Fig. 3(b). Additional experiments for the SN hydrogel, which are not reported here, show that the difference between loading and unloading curves when the stretch rate was changed by a factor of ten was also less than 1 kPa. Thus *relative* to the *S-λ* response of the DN hydrogel, the *S-λ* response of the SN hydrogel may be idealized to be essentialy rate-independent, and we shall make such an idealization in developing our constitutive theory.

Fig. 4a shows stress-stretch curves for the DN hydrogel at four different stretch rates $\dot\lambda$ ranging from 0.4/min to 35.3/min. Thus, in addition to the striking Mullins-type effect, the DN hydrogel also shows a significant stretch-rate sensitivity. It is important to note
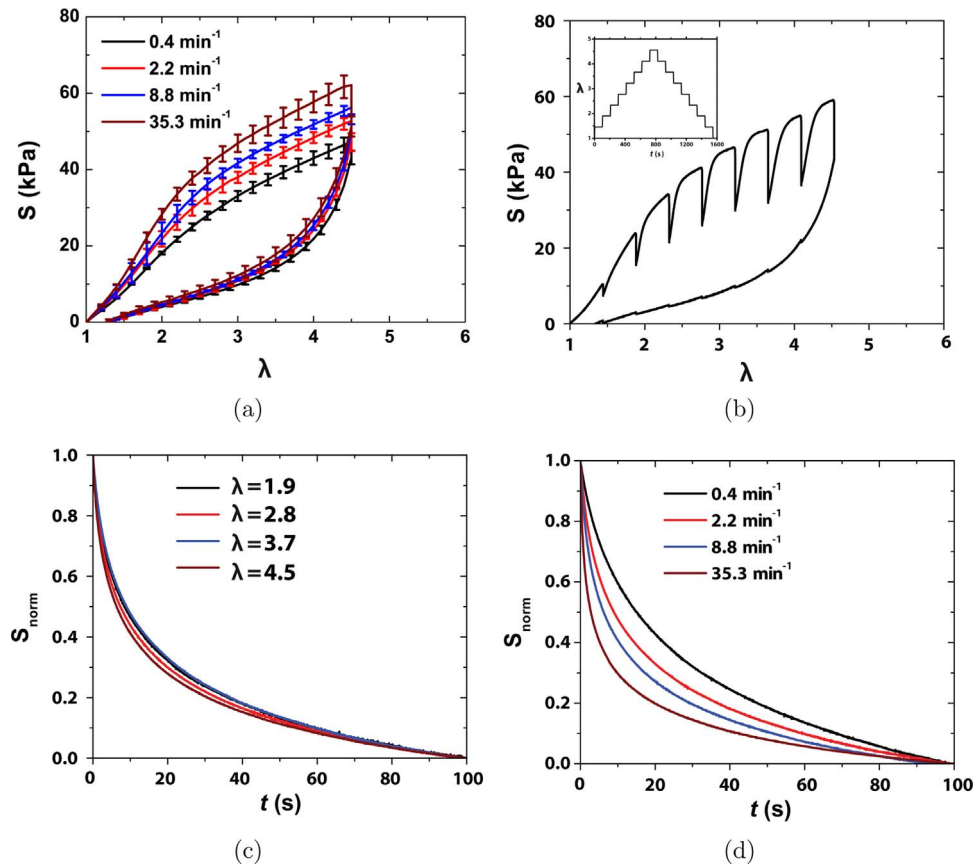


**Fig. 4.** Time-dependent mechanical behavior of DN hydrogel: (a) $S$ versus $\lambda$ response at stretch rates ranging from 0.4/min to 35.3/min. (b) $S$ versus $\lambda$ curves with interrupted stress-relaxation experiments. (c) $S_{norm}(t) \overset{\text{def}}{=} (S(t) - S_\infty)/(S(0) - S_\infty)$ is essentially independent of the level of stretch in the range $\lambda \in [1, 4.5]$ for a test conducted at a nominal stretch rate of 8.8/min. (d) $S_{norm}(t)$ is dependent on the stretch-rate in the range $\dot\lambda \in [0.4, 35.3]$/min.

that while the $S$ versus $\lambda$ response is rate-sensitive during loading, *the rate-sensitivity during unloading is small and almost negligible*. The rate-dependence of the loading portion of the curve arises mainly due to the kinetic rupturing of the ionically crosslinked alginate network. As the sample is stretched the ionic bonds in the alginate network rupture, and the experiments show that this energy dissipation mechanism is rate-dependent. In contrast, during unloading — that is, as the stretch is reduced — there is no additional disruption of the alginate network, and therefore the unloading response is *essentially rate-independent*, an assumption that we will adopt in our efforts at modeling the response of the DN hydrogel. Further, Fig. 4(a) shows that the DN hydrogel also exhibits some permanent set upon unloading, but the permanent set is relatively *small* compared to the overall stretch levels. In our efforts at modeling the response of DN hydrogels, *we shall **neglect** the effects of such inelastic deformation*. We leave an inclusion of such effects to a future endeavor.

To further investigate the rate-sensitivity of the DN hydrogel we conducted sequential stress-relaxation experiments in which we stretched the sample to various stretches $\lambda = 1.44, 1.88, 2.32, 2.77, 3.22, 3.64, 4.10$ and $4.5$ at a given nominal stretch rate of 8.8/ min, interspersed with a hold period of 100 s, and also repeated the hold periods during unloading. This stretch history is shown schematically in the inset of Fig. 4(b). This figure also shows the resulting $S$ versus $\lambda$ curve. Similar to the asymmetric rate sensitivity discussed with respect to Fig. 4(a), the DN hydrogel shows stress-relaxation during loading, but not during unloading.

During each stretch-hold period of 100 s during the loading phase, the engineering stress $S(t)$ gradually decreases to reach an asymptotic value of $S_\infty$. Let

$$S_{\mathrm{norm}}(t) \overset{\mathrm{def}}{=} \frac{(S(t) - S_\infty)}{(S(0) - S_\infty)},$$

denote a normalized value of $S(t)$ during each stress-relaxation phase. We studied the variation of the normalized stress $S_{\mathrm{norm}}(t)$ as function of stretch at various stretch rates, and found that $S_{\mathrm{norm}}(t)$ was essentially independent of the level of stretch in the range $\lambda \in [1, 4.5]$, cf. Fig. 4(c), but that it was very dependent on the stretch-rate in the range $\dot{\lambda} \in [0.4, 35.3]$/min that we studied experimentally, cf. Fig. 4(d).

Finally, to distinguish between the rate-dependent and the rate-independent aspects of the stress-stretch response of the DN hydrogel we performed several tension tests on identical samples at various stretch rates in the range $\dot{\lambda} \in [0.4, 35.3]$/min, with
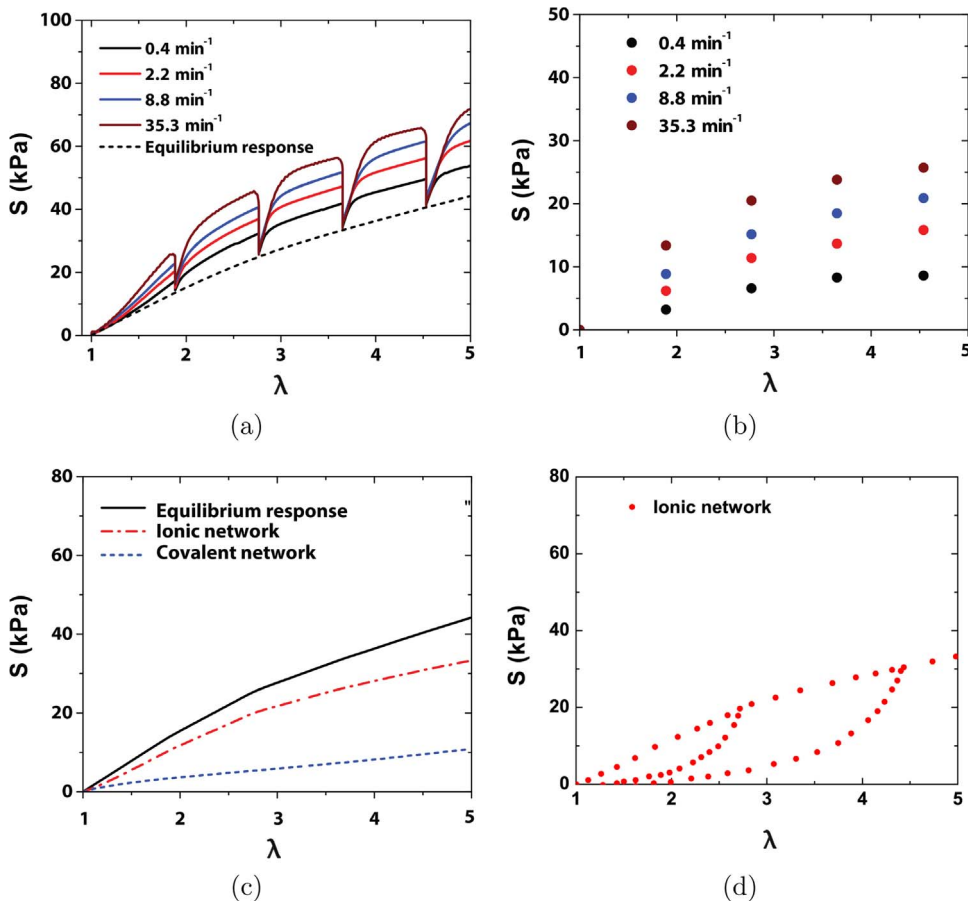


**Fig. 5.** (a) $S$ versus $\lambda$ response for different stretch rates with relaxation holdings. The dashed line is identified as the equilibrium response of the material. (b) viscoelasticity part of $S$-$\lambda$ curves for different stretch rates. (c) Separating the response of the covalent network and the ionic network. (d) The complete response of the ionic network.

interrupted periods of stress-relaxation; cf. Fig. 5a. As shown in this figure, the engineering stress $S$ during each hold period decreases to a limiting value. These limiting values of stress at each stretch level represent a purely elastic — or an *equilibrum reponse* — of the DN hydrogel. By subtracting this "equilibrium response" from the total stress $S$, we can obtain the purely rate-dependent contribution to the stress in the DN hydrogel; this is shown in Fig. 5(b). Finally, by subtracting the $S$-$\lambda$ curve for the SN hydrogel, the dashed blue line (cf. Fig. 3a) from the "equilibrium response" (the solid black line), the elastic contribution from the alginate network can be estimated; this is shown by the dash-dot red line in Fig. 5(c).[2] Recall that the unloading response of the DN hydrogel is essentially rate-independent. Thus by appending the unloading curves from various stretches to the dash-dot redline of Fig. 5(c), the essentially rate-independent loading-unloading curves — showing a large Mullins-type effect — for the DN hydrogel may be constructed, as shown in Fig. 5(d).

In summary, the DN hydrogel shows three major characteristic responses which are different from conventional elastomeric materials:

(i) a large Mullins-type effect which manifests itself in hysteresis during loading and unloading;
(ii) an asymmetric rate-sensitive response during loading and unloading; and
(iii) a stretch-independent but stretch-rate dependent stress-relaxation behavior.

In Section 3 we summarize our large deformation viscoelasticity theory, and in Section 4 we specialize this theory to model the DN hydrogel which we have studied experimentally in this section.

## 3. Theory

Our theory for the double network hydrogels is a specialized version of a more-general theory viscoelasticity theory based on a Kröner-type multimechanism, multiplicative decomposition of the deformation gradient $\mathbf{F}$ of the form,

$$\mathbf{F} = \mathbf{F}^{e(\alpha)}\mathbf{F}^{v(\alpha)}, \quad \alpha = 1,\ldots,M, \tag{3.1}$$

in which $\alpha$ indexes a micromechanism which governs the response of a multiple-network gel.[3] Each micromechanism is characterized by a constant (positive-valued scalar) *volume fraction* $\chi^{(\alpha)}$ which satisfies the constraint,

$$\sum_\alpha \chi^{(\alpha)} = 1 - \chi^{\text{solv}}, \tag{3.2}$$

where $\chi^{\text{solv}}$ is a constant volume fraction of solvent in the gel.

Our theory, which is developed in detail in Appendix A, relates the following basic fields:[4]

| | |
|---|---|
| $\mathbf{x} = \boldsymbol{\chi}(\mathbf{X}, t)$, | motion; |
| $\mathbf{F} = \nabla\boldsymbol{\chi}, \quad J = \det\mathbf{F} > 0$, | deformation gradient; |
| $\mathbf{C} = \mathbf{F}^{\mathsf{T}}\mathbf{F}$, | right Cauchy-Green tensor; |
| $\mathbf{B} = \mathbf{FF}^{\mathsf{T}}$, | left Cauchy-Green tensor; |
| $\overline{\mathbf{F}} = J^{-1/3}\mathbf{F}, \quad \det\overline{\mathbf{F}} = 1$, | isochoric part of $\mathbf{F}$; |
| $\overline{\mathbf{C}} = \overline{\mathbf{F}}^{\mathsf{T}}\overline{\mathbf{F}}, \quad \det\overline{\mathbf{C}} = 1$, | isochoric part of $\mathbf{C}$; |
| $\overline{\mathbf{B}} = \overline{\mathbf{F}}\,\overline{\mathbf{F}}^{\mathsf{T}}, \quad \det\overline{\mathbf{B}} = 1$, | isochoric part of $\mathbf{B}$; |
| $\mathcal{I}_{\overline{\mathbf{C}}}$ and $\mathcal{I}_{\overline{\mathbf{B}}}$, | list of principal invariants of $\overline{\mathbf{C}}$ and $\overline{\mathbf{B}}$; |
| $\bar{\lambda} = \sqrt{\operatorname{tr}\overline{\mathbf{C}}/3} = \sqrt{\operatorname{tr}\overline{\mathbf{B}}/3}$, | effective distortional stretch; |
| $\chi^{(\alpha)}(\mathbf{X})$, | volume fraction of the $\alpha$th micromechanism/ "phase"; |
| $\mathbf{F} = \mathbf{F}^{e(\alpha)}\mathbf{F}^{v(\alpha)} \quad \alpha = 1,\ldots,M$, | multimechanism multiplicative decomposition of $\mathbf{F}$; |
| $\mathbf{F}^{v(\alpha)}, \quad J^{v(\alpha)} = \det\mathbf{F}^{v(\alpha)} = 1$, | isochoric viscous distortion for the $\alpha$th micromechanism; |
| $\mathbf{F}^{e(\alpha)}, \quad J^{e(\alpha)} = \det\mathbf{F}^{e(\alpha)} > 0$, | elastic distortion for the $\alpha$th micromechanism; |
| $J = J^{e(\alpha)}$; | |
| $\mathbf{C}^{e(\alpha)} = \mathbf{F}^{e(\alpha)\mathsf{T}}\mathbf{F}^{e(\alpha)}$, | elastic right Cauchy-Green tensors; |
| $\mathbf{B}^{e(\alpha)} = \mathbf{F}^{e(\alpha)}\mathbf{F}^{e(\alpha)\mathsf{T}}$, | elastic left Cauchy-Green tensors; |
| $\overline{\mathbf{F}}^{e(\alpha)} = (J^{e(\alpha)})^{-1/3}\mathbf{F}^{e(\alpha)}, \quad \det\overline{\mathbf{F}}^{e(\alpha)} = 1$, | isochoric part of $\mathbf{F}^{e(\alpha)}$; |

---

[2] Please refer to the online version of this article for color coding in various graphs.

[3] A theory based on a decomposition of the form (3.1) has also been successfully used for modeling the behavior of glassy polymers, both below and above their glass transition temperatures (cf., e.g., Boyce et al., 2000; Anand et al., 2009; Ames et al., 2009; Srivastava et al., 2010a, 2010b).

[4] Notation: We use standard notation of modern continuum mechanics (Gurtin et al., 2010). Specifically: $\nabla$ and Div denote the gradient and divergence with respect to the material point $\mathbf{X}$ in the reference configuration, and $\Delta = \operatorname{Div}\nabla$ denotes the referential Laplace operator; grad, div, and divgrad denote these operators with respect to the point $\mathbf{x} = \boldsymbol{\chi}(\mathbf{X}, t)$ in the deformed body; a superposed dot denotes the material time-derivative. Throughout, we write $\mathbf{F}^{e-1} = (\mathbf{F}^e)^{-1}$, $\mathbf{F}^{e-\mathsf{T}} = (\mathbf{F}^e)^{-\mathsf{T}}$, etc. We write trA, symA, skwA, $\mathbf{A}_0$, and $\operatorname{sym}_0\mathbf{A}$ respectively, for the trace, symmetric, skew, deviatoric, and symmetric-deviatoric parts of a tensor $\mathbf{A}$. Also, the inner product of tensors $\mathbf{A}$ and $\mathbf{B}$ is denoted by $\mathbf{A}: \mathbf{B}$, and the magnitude of $\mathbf{A}$ by $|\mathbf{A}| = \sqrt{\mathbf{A}:\mathbf{A}}$.

$$\overline{\mathbf{C}}^{e(\alpha)} = \overline{\mathbf{F}}^{e(\alpha)\top}\overline{\mathbf{F}}^{e(\alpha)}, \quad \det \overline{\mathbf{C}}^{e(\alpha)} = 1,$$ isochoric elastic right Cauchy-Green tensors;

$$\mathcal{I}_{\overline{\mathbf{C}}^{e(\alpha)}},$$ list of principal invariants of $\overline{\mathbf{C}}^{e(\alpha)}$;

$$\mathbf{F}^{e(\alpha)} = \mathbf{R}^{e(\alpha)}\mathbf{U}^{e(\alpha)} = \mathbf{V}^{e(\alpha)}\mathbf{R}^{e(\alpha)},$$ polar decompositions of $\mathbf{F}^{e(\alpha)}$;

$$\mathbf{U}^{e(\alpha)} = \sum_{i=1}^{3} \lambda_i^{e(\alpha)} \mathbf{r}_i^{e(\alpha)} \otimes \mathbf{r}_i^{e(\alpha)},$$ spectral decomposition of $\mathbf{U}^{e(\alpha)}$;

$$\mathbf{V}^{e(\alpha)} = \sum_{i=1}^{3} \lambda_i^{e(\alpha)} \mathbf{l}_i^{e(\alpha)} \otimes \mathbf{l}_i^{e(\alpha)},$$ spectral decomposition of $\mathbf{V}^{e(\alpha)}$;

$$\mathbf{E}^{e(\alpha)} = \sum_{i=1}^{3} (\ln \lambda_i^{e(\alpha)}) \mathbf{r}_i^{e(\alpha)} \otimes \mathbf{r}_i^{e(\alpha)},$$ logarithmic elastic strain;

$$\mathbf{E}_{\mathrm{H}}^{e(\alpha)} = \mathbf{R}^{e(\alpha)}\mathbf{E}^{e(\alpha)}\mathbf{R}^{e(\alpha)\top} = \sum_{i=1}^{3} (\ln \lambda_i^{e(\alpha)}) \mathbf{l}_i^{e(\alpha)} \otimes \mathbf{l}_i^{e(\alpha)},$$ spatial logarithmic elastic strain;

$$\mathbf{T} = \sum_{\alpha} \chi^{(\alpha)} \mathbf{T}^{(\alpha)},$$ Cauchy stress;

$$\mathbf{T}^{e(\alpha)} = J^{e(\alpha)}\mathbf{F}^{e(\alpha)-1}\mathbf{T}^{(\alpha)}\mathbf{F}^{e(\alpha)-\top},$$ elastic second Piola stress for the $\alpha$th micromechanism;

$$\mathbf{M}^{e(\alpha)} = \mathbf{C}^{e(\alpha)}\mathbf{T}^{e(\alpha)},$$ Mandel stress for the $\alpha$th micromechanism;

$$\mathbf{T}_{\mathrm{R}} = J\mathbf{T}\mathbf{F}^{-\top},$$ Piola stress;

$$\psi_{\mathrm{R}},$$ free energy density per unit reference volume.

**Remark.** A feature of the multimechanism Kroner-type decomposition $\mathbf{F} = \mathbf{F}^{e(\alpha)}\mathbf{F}^{v(\alpha)}$ (with $\det \mathbf{F}^{v(\alpha)} = 1$) is that $J^{e(\alpha)} = J$ for all $\alpha$. In the specialized constitutive equations to be considered below, we will associate $J$ with only one micromechanism, while all other micromechanisms will be taken to be elastically and plastically *isochoric*.

In order to account for the microstructural changes that alter the number of crosslinks in the material during deformation, we introduce a list $M$ scalar internal variables, one for each micromechanism,

$$\vec{\xi} = \{\xi^{(1)}, \ldots, \xi^{(M)}\}.$$

Also, to account for important aspects of the microstructural changes which result in changes in the resistance to viscous flow during deformation we introduce another list

$$\vec{s} = \{s^{(1)}, \ldots, s^{(M)}\}.$$

We also limit our attention to situations under which the material may be idealized to be *isotropic*. Accordingly, all constitutive functions considered below are presumed to be isotropic in character. Finally, when convenient, we shall use the shorthand

$$\sum_{\alpha} = \sum_{\alpha=1}^{M}, \tag{3.3}$$

1. **Free energy**:

   We assume a free energy in the separable form,

$$\psi_{\mathrm{R}} = \chi^{\mathrm{solv}}\psi_{\mathrm{R}}^{\mathrm{solv}} + \sum_{\alpha} \chi^{(\alpha)}\psi_{\mathrm{R}}^{(\alpha)}(\mathcal{I}_{\mathbf{C}^{e(\alpha)}}, \xi^{(\alpha)}). \tag{3.4}$$

   Here, $\psi_{\mathrm{R}}^{\mathrm{solv}}$ represents a constant free energy contribution from the solvent, and $\psi_{\mathrm{R}}^{(\alpha)}$ represents the contribution to the free energy from the $\alpha$th micromechanism, with $\mathcal{I}_{\mathbf{C}^{e(\alpha)}}$ represents a list of the principal invariants of $\mathbf{C}^{e(\alpha)}$.

2. **Elastic second Piola stress. Mandel Stress. Cauchy stress**:

   For each micromechanism the elastic second Piola stress is given by

$$\mathbf{T}^{e(\alpha)} = 2\frac{\partial \psi_{\mathrm{R}}^{(\alpha)}(\mathcal{I}_{\mathbf{C}^{e(\alpha)}}, \xi^{(\alpha)})}{\partial \mathbf{C}^{e(\alpha)}}, \tag{3.5}$$

   the symmetric Mandel stresses by

$$\mathbf{M}^{e(\alpha)} = \mathbf{C}^{e(\alpha)}\mathbf{T}^{e(\alpha)}, \tag{3.6}$$

   and the contributions $\mathbf{T}^{(\alpha)}$ to the Cauchy stress $\mathbf{T}$ (recalling that $J^{e(\alpha)} = J$) by

$$\mathbf{T}^{(\alpha)} = J^{-1}\left(2\mathbf{F}^{e(\alpha)}\frac{\partial \psi_{\mathrm{R}}^{(\alpha)}(\mathcal{I}_{\mathbf{C}^{e(\alpha)}}, \xi^{(\alpha)})}{\partial \mathbf{C}^{e(\alpha)}}\mathbf{F}^{e(\alpha)\top}\right). \tag{3.7}$$

   The total Cauchy stress $\mathbf{T} = \sum_{\alpha}\chi^{(\alpha)}\mathbf{T}^{(\alpha)}$ is then given by

$$\mathbf{T} = \sum_{\alpha} \chi^{(\alpha)}J^{-1}\left(2\mathbf{F}^{e(\alpha)}\frac{\partial \psi_{\mathrm{R}}^{(\alpha)}(\mathcal{I}_{\mathbf{C}^{e(\alpha)}}, \xi^{(\alpha)})}{\partial \mathbf{C}^{e(\alpha)}}\mathbf{F}^{e(\alpha)\top}\right). \tag{3.8}$$

3. **Evolution equation for $\mathbf{F}^{v(\alpha)}$**:

The evolution equation for each $\mathbf{F}^{v(\alpha)}$ is

$$\dot{\mathbf{F}}^{v(\alpha)} = \mathbf{D}^{v(\alpha)}\mathbf{F}^{v(\alpha)}, \quad \mathbf{F}^{v(\alpha)}(\mathbf{X}, 0) = \mathbf{1}, \tag{3.9}$$

with the viscous stretching given by

$$\mathbf{D}^{v(\alpha)} = \dot{\bar{\gamma}}^{v(\alpha)}\left(\frac{\mathbf{M}_0^{e(\alpha)}}{2\bar{\tau}^{(\alpha)}}\right), \tag{3.10}$$

where

$$\bar{\tau}^{(\alpha)} \stackrel{\text{def}}{=} \frac{1}{\sqrt{2}}|\mathbf{M}_0^{e(\alpha)}| \tag{3.11}$$

defines an *equivalent shear stress* for each $\alpha$, and

$$\dot{\bar{\gamma}}^{v(\alpha)} \stackrel{\text{def}}{=} \sqrt{2}|\mathbf{D}^{v(\alpha)}|, \tag{3.12}$$

is an *equivalent viscous shear strain rate*.

Let

$$\Lambda^{(\alpha)} = (\mathbf{C}^{e(\alpha)}, s^{(\alpha)}, \xi^{(\alpha)}) \tag{3.13}$$

denote a list of constitutive variables. Then, for given $\bar{\tau}^{(\alpha)}$ and $\Lambda^{(\alpha)}$, the equivalent viscous shear strain rate $\dot{\bar{\gamma}}^{v(\alpha)}$ is obtained by solving a scalar strength relation

$$\bar{\tau}^{(\alpha)} = Y^{(\alpha)}(\Lambda^{(\alpha)}, \dot{\bar{\gamma}}^{v(\alpha)}), \tag{3.14}$$

where the strength function $Y^{(\alpha)}(\dot{\bar{\gamma}}^{v(\alpha)}, \Lambda^{(\alpha)})$ is an isotropic function of its arguments. We assume that

$$Y^{(\alpha)}(\dot{\bar{\gamma}}^{v(\alpha)}, \Lambda^{(\alpha)}) \text{ is a positive–valued strictly increasing function of } \dot{\bar{\gamma}}^{v(\alpha)}, \tag{3.15}$$

so that

(1) the viscous dissipation inequality

$$Y^{(\alpha)}\dot{\bar{\gamma}}^{v(\alpha)} > 0 \quad \text{for} \quad \dot{\bar{\gamma}}^{v(\alpha)} > 0,$$

is satisfied, and that

(2) for each fixed $\Lambda^{(\alpha)}$, the function $Y^{(\alpha)}(\dot{\bar{\gamma}}^{v(\alpha)}, \Lambda^{(\alpha)})$ is *invertible*.

Hence,

$$\dot{\bar{\gamma}}^{v(\alpha)} = f^{(\alpha)}(\bar{\tau}^{(\alpha)}, \Lambda^{(\alpha)}) \geq 0. \tag{3.16}$$

4. **Evolution equations for the internal variables $\xi^{(\alpha)}$ and $s^{(\alpha)}$**:

We shall elaborate on evolution equations for the internal variables $\xi^{(\alpha)}$ and $s^{(\alpha)}$ when we specialize our constitutive theory in Section 4.

5. **Total dissipation rate**:

The total rate of dissipation per unit reference volume is

$$\mathcal{D} = \sum_{\alpha} \chi^{(\alpha)} Y^{(\alpha)}\dot{\bar{\gamma}}^{v(\alpha)} - \sum_{\alpha} \chi^{(\alpha)} \frac{\partial \psi_{\mathrm{R}}^{(\alpha)}(\mathbf{C}^{e(\alpha)}, \xi^{(\alpha)})}{\partial \xi^{(\alpha)}}\dot{\xi}^{(\alpha)} \geq 0, \tag{3.17}$$

with contributions from both the viscous dissipation and how the evolution of the internal variables $\xi^{(\alpha)}$ changes the free energy of the body.

## 4. Specialization of the constitutive equations

The theory presented in the previous subsection is quite general. Here, in order to model the response of double-network gels, we use three micromechanisms, $\alpha = 1, 2, 3$. To fix ideas, Fig. 6 shows a rheological spring-dashpot model for the three micromechanisms model that we shall elaborate on below.

Specifically:
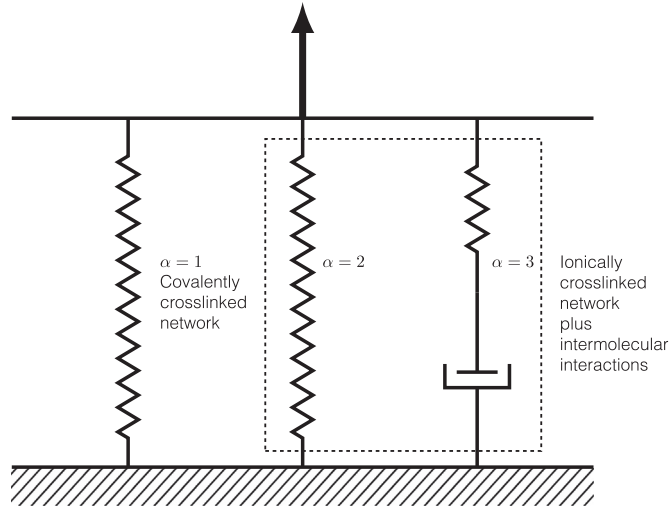
**Fig. 6.** Rheological model for double-network gels.

(i) The first micromechanism, $\alpha = 1$, is taken to represent a covalently-crosslinked network with long chains.
   - *We limit our attention to circumstances under which the covalent crosslinks in this network do not to rupture; that is we do not attempt to model fracture of the gel.*
   We also do not associate any viscous deformation with this network, and accordingly set $\mathbf{F}^{v(1)} = \mathbf{1}$.
(ii) The second and third micromechanisms, $\alpha = 2$ and $\alpha = 3$, are taken to **together** represent the ionically-crosslinked network with short chains plus all intermolecular interactions. Accordingly, we set the volume fraction $\chi^{(3)}$ to be equal to $\chi^{(2)}$,

$$\chi^{(2)} = \chi^{(3)}, \tag{4.1}$$

*with the sum of the two equal to the volume fraction of the ionic network in the double-network hydrogel.* The ionic crosslinks, which are conceptually represented by network $\alpha = 2$, may rupture — resulting in distributed internal microdamage and dissipation due to such microdamage, but we do not directly associate any viscous deformation with this network, and accordingly set $\mathbf{F}^{v(2)} = \mathbf{1}$. That is, the micromechanism $\alpha = 2$ will be used to model the rate-independent elastic response of the short-chain network with a concommitant Mullins-type phenomena. All viscous effects in the material will be associated with the third micromechanism, $\alpha = 3$, which is presumed to also account for an elastic resistance due to intermolecular energetic bond-stretching. Accordingly for this mechanism we prescribe a suitable evolution equation for $\mathbf{F}^{v(3)}$ to describe rate-dependent dissipative phenomena.

Since $\mathbf{F}^{v(1)} = \mathbf{1}$ and $\mathbf{F}^{v(2)} = \mathbf{1}$, by assumption, we have

$$\overline{\mathbf{C}}^{e(1)} = \overline{\mathbf{C}}, \quad \mathcal{I}_{\overline{\mathbf{C}}^{e(1)}} = \mathcal{I}_{\overline{\mathbf{C}}}, \quad \text{and} \quad \overline{\mathbf{C}}^{e(2)} = \overline{\mathbf{C}}, \quad \mathcal{I}_{\overline{\mathbf{C}}^{e(2)}} = \mathcal{I}_{\overline{\mathbf{C}}}.$$

We take the free energy to be given in the separable form

$$\psi_{\mathrm{R}} = \chi^{\mathrm{solv}}\psi_{\mathrm{R}}^{\mathrm{solv}} + \chi^{(1)}\psi_{\mathrm{R}}^{(1)}(\mathcal{I}_{\overline{\mathbf{C}}}) + \chi^{(2)}\psi_{\mathrm{R}}^{(2)}(\mathcal{I}_{\overline{\mathbf{C}}}, \xi^{(2)}) + \chi^{(3)}\psi_{\mathrm{R}}^{(3)}(\mathcal{I}_{\mathbf{C}^{e(3)}}, \xi^{(3)}). \tag{4.2}$$

That is, we assume that

- the free energies for the micromechanisms $\alpha = 1, 2$ do not depend on the corresponding volumetric elastic contributions, and that *all volumetric elastic contributions are accounted for the in the free energy for the intermolecular mechanism labeled $\alpha = 3$.*
- Also, since the first micromechanism, $\alpha = 1$, has been taken to represent a covalently-crosslinked network for which the crosslinks are presumed not to rupture, we have assumed that the free energy for this micromechanism does not involve an internal variable $\xi^{(1)}$, and depends only on the list of invariants $\mathcal{I}_{\overline{\mathbf{C}}}$ of $\overline{\mathbf{C}}$.

*4.1. Constitutive equations for micromechanism $\alpha = 1$*

For the network with long chains in which the covalent crosslinks are presumed not to rupture and for which there is no viscous flow, we take $\psi_{\mathrm{R}}^{(1)}$ to depend only on the first invariant of $\overline{\mathbf{C}}$,

$$I_1 = \mathrm{tr}\,\overline{\mathbf{C}},$$

in the Gent (1996) form,

$$\psi_R^{(1)} = -\frac{1}{2}C^{(1)}I_m^{(1)}\ln\left(1 - \frac{I_1 - 3}{I_m^{(1)}}\right).$$

(4.3)

Here,

$$C^{(1)} > 0, \quad I_m^{(1)},$$

are two material parameters in which $I_m^{(1)}$ sets a bound on the maximum possible value of $I_1$ (i.e., $0 \le (I_1 - 3)/I_m^{(1)} < 1$).

From (4.3) and (3.7) the contribution to the Cauchy stress form the first micromechanism is

$$\mathbf{T}^{(1)} = J^{-1}G^{(1)}\overline{\mathbf{B}}_0, \quad G^{(1)} \stackrel{\text{def}}{=} C^{(1)}\left(1 - \frac{I_1 - 3}{I_m^{(1)}}\right)^{-1},$$

(4.4)

with $\mathbf{T}^{(1)}$ deviatoric.

**Remark.** As an alternative to the Gent form of the free energy (4.3), introducing an *effective distortional stretch* defined by

$$\bar{\lambda} \stackrel{\text{def}}{=} \sqrt{\frac{\mathrm{tr}\overline{\mathbf{C}}}{3}},$$

(4.5)

one may also use a free energy in the Arruda and Boyce (1993) form,

$$\psi_R^{(1)} = G_0^{(1)}(\lambda_L^{(1)})^2\left[\left(\frac{\bar{\lambda}}{\lambda_L^{(1)}}\right)\beta^{(1)} + \ln\left(\frac{\beta^{(1)}}{\sinh\beta^{(1)}}\right) - \left(\frac{1}{\lambda_L^{(1)}}\right)\beta_0^{(1)} - \ln\left(\frac{\beta_0^{(1)}}{\sinh\beta_0^{(1)}}\right)\right],$$

(4.6)

in which

$$G_0^{(1)} \stackrel{\text{def}}{=} N^{(1)}k_B\vartheta, \quad \beta^{(1)} \stackrel{\text{def}}{=} \mathcal{L}^{-1}\left(\frac{\bar{\lambda}}{\lambda_L^{(1)}}\right), \quad \beta_0^{(1)} \stackrel{\text{def}}{=} \mathcal{L}^{-1}\left(\frac{1}{\lambda_L^{(1)}}\right),$$

(4.7)

with $\mathcal{L}^{-1}$ the inverse of the Langevin function $\mathcal{L}(x) = \coth(x) - (x)^{-1}$. Here, (i) $N^{(1)}$ denote the number of polymer chains per unit volume of the refrence configuration; (ii) $n^{(1)}$ the number of links per chain; and (iii) $\lambda_L^{(1)}$ defined by $\lambda_L^{(1)} \stackrel{\text{def}}{=} \sqrt{n^{(1)}}$, the locking stretch for the first network.

While the free energy (4.6) may appear to be more fundamentally motivated because it is based on statistical mechanical considerations, there is a conceptual difficulty with using statistical-mechanical ideas here. This is because of the presence of the second network, the chains in the first network do not have sufficient freedom to sample all possible molecular conformations, as visualized in the statistical-mechanical models of rubber elasticity. It is for this reason that we employ a simple *phenomenological* form for the free energy function due to Gent (1996). The Gent model has been shown to yield predictions for the stress-strain response similar to the entropic-network model of Arruda and Boyce, by Boyce (1996).

### 4.2. Constitutive equations for micromechanism $\alpha = 2$

The second micromechanism is taken to represent a portion of the response the ionically crosslinked network. We take $\psi_R^{(2)}$ to depend on $I_1 = \mathrm{tr}\overline{\mathbf{C}}$ in the Gent (1996) form,

$$\psi_R^{(2)} = -\frac{1}{2}C^{(2)}I_m^{(2)}\ln\left(1 - \frac{I_1 - 3}{I_m^{(2)}}\right),$$

(4.8)

with two material parameters

$$C^{(2)} > 0 \quad \text{and} \quad I_m^{(2)},$$

(4.9)

in which $I_m^{(2)}$ sets a bound on the maximum possible value of $I_1$ (i.e., $0 \le (I_1 - 3)/I_m^{(2)} < 1$).

The rupture of the ionic crosslinks leads to a stretch-softening phenomenon similar to the well-known *Mullins effect* (cf., e.g., Mullins, 1969) in natural and synthetic elastomers. Numerous models have been proposed to model such stretch-softening of elastomeric materials (cf., e.g., Marckmann et al., 2002; Qi and Boyce, 2004; Chagnon et al., 2006; Cho et al., 2013, and the references to the literature in these papers). Specifically, Marckmann et al. (2002) proposed that the Mullins effect was caused by the disruption of the crosslinks in a network, and accordingly suggested that the microdamage process results in an increase in the mean distance between crosslinks, i.e. the mean length of chains increases, and a concommitant decrease in the number of chains per unit of volume. Guided by the physical ideas of Marckmann et al. (2002) and Chagnon et al. (2006), and the models of Boyce and co-workers (Qi and Boyce, 2004; Cho et al., 2013) on network alteration, we construct a simple model for the microdamage processes for the double-network hydrogels under consideration here.

Recall the definition Eq. (4.5) for the *effective distortional stretch*, viz.

$$\bar{\lambda} \stackrel{\text{def}}{=} \sqrt{\frac{\mathrm{tr}\,\overline{\mathbf{C}}}{3}}.$$

(4.10)

Let

$$\bar{\lambda}_{\max}(t) \overset{\text{def}}{=} \max_{\zeta \in [0,t]} [\bar{\lambda}(\zeta)] \tag{4.11}$$

represent the *maximum* effective distortional elastic stretch that the material has been locally subjected to over its history $\zeta \in [0, t]$. Following Marckmann et al. (2002) we presume that microscale damage is actuated when the chains are stretched above the maximum effective stretch ever applied to the network. To model the microdamage caused by the the disruption of the ionic crosslinks, we take the internal variable $\xi^{(2)}$ to be identically equal to $\bar{\lambda}_{\max}$,

$$\xi^{(2)} \equiv \bar{\lambda}_{\max}, \tag{4.12}$$

and assume that the moduli $C^{(2)}$ and $I_m^{(2)}$ in (4.8) are functions of $\bar{\lambda}_{\max}$ of the form

$$C^{(2)} = C_0^{(2)} f(\bar{\lambda}_{\max}) \quad f(1) = 1, \, I_m^{(2)} = I_{m,0}^{(2)} \, g(\bar{\lambda}_{\max}), \quad g(1) = 1, \tag{4.13}$$

where $C_0^{(2)}$ and $I_{m,0}^{(2)}$ are the initial values of $C^{(2)}$ and $I_m^{(2)}$, with the functions $f(\bar{\lambda}_{\max})$ and $g(\bar{\lambda}_{\max})$ chosen such that $C^{(2)}$ decreases while $I_m^{(2)}$ increases as $\bar{\lambda}_{\max}$ increases. Further we require that at any value of $\bar{\lambda}_{\max}$,

$$f(\bar{\lambda}_{\max}) \, g(\bar{\lambda}_{\max}) \equiv 1. \tag{4.14}$$

In particular, we assume that

$$f(\bar{\lambda}_{\max}) = (p + (1 - p)\bar{\lambda}_{\max})^{-q}, \quad g(\bar{\lambda}_{\max}) = (p + (1 - p)\bar{\lambda}_{\max})^q, \tag{4.15}$$

with

$$p > 0, \quad q > 0. $$

From (4.8) and (3.7) we find that the contribution to the Cauchy stress form the second micromechanism is

$$\mathbf{T}^{(2)} = J^{-1} G^{(2)} \overline{\mathbf{B}}_0, \quad \text{with} \quad G^{(2)} \overset{\text{def}}{=} C^{(2)} \left( 1 - \frac{I_1 - 3}{I_m^{(2)}} \right)^{-1}, \tag{4.16}$$

with $\mathbf{T}^{(2)}$ *deviatoric*.

### 4.3. Constitutive equations for micromechanism $\alpha = 3$

For the intermolecular energetic bond-stretching interactions, instead of using the invariants $\mathcal{I}_{\mathbf{C}^e}$, recalling the spectral representation

$$\mathbf{C}^e = \sum_{i=1}^{3} \omega_i^e \, \mathbf{r}_i^e \otimes \mathbf{r}_i^e \quad \text{with} \quad \omega_i^e = \lambda_i^{e2}, \tag{4.17}$$

where $(\mathbf{r}_1^e, \mathbf{r}_2^e, \mathbf{r}_2^e)$ are the orthonormal eigenvectors of $\mathbf{C}^e$ and $\mathbf{U}^e$, and $(\lambda_1^e, \lambda_2^e, \lambda_3^e)$ are the positive eigenvalues of $\mathbf{U}^e$, we take free energy $\psi_R$ to be alternatively expressed in terms of the principal stretches $(\lambda_1^e, \lambda_2^e, \lambda_3^e)$. Further, with

$$E_i^e \overset{\text{def}}{=} \ln \lambda_i^e \tag{4.18}$$

defining the principal values of the logarithmic elastic strain

$$\mathbf{E}^e \overset{\text{def}}{=} \ln \mathbf{U}^e = \sum_{i=1}^{3} E_i^e \mathbf{r}_i^e \otimes \mathbf{r}_i^e, \tag{4.19}$$

we take the free energy in the form

$$\psi_R = \psi_R (E_1^e, E_2^e, E_3^e). \tag{4.20}$$

Thus, with $\mathbf{E}^{e(3)}$ the logarithmic elastic strain for the intermolecular mechanism $\alpha = 3$ defined as above, we take $\psi_R^{(3)}$ to be given in the specific form (Anand, 1979, 1986),

$$\psi_R^{(3)}(\mathbf{E}^{e(3)}, \xi^{(3)}) = \left[ G^{(3)}((E_1^{e(3)})^2 + (E_2^{e(3)})^2 + (E_3^{e(3)})^2) + \frac{1}{2}(K - (2/3)G)(E_1^{e(3)} + E_2^{e(3)} + E_3^{e(3)})^2 \right], \tag{4.21}$$

where the parameters

$$G^{(3)} > 0, \quad K > 0, \tag{4.22}$$

are the shear modulus and bulk modulus, respectively, possibly dependent on an internal varaible $\xi^{(3)}$; a dependence which we will discuss shortly in what follows.

Using the relations given in Section 3, the Cauchy stress for micromechanism $\alpha = 3$ is,

$$\mathbf{T}^{(3)} = (J^{e(3)})^{-1} \mathbf{R}^{e(3)} \mathbf{M}^{e(3)} \mathbf{R}^{e(3)\top}, \tag{4.23}$$

with $\mathbf{M}^{e(3)}$ the corresponding Mandel stress given by

$$\mathbf{M}^{e(3)} = 2G^{(3)} \mathbf{E}_0^{e(3)} + K \, (\text{tr} \mathbf{E}^{e(3)}) \mathbf{1}. \tag{4.24}$$

Substituting (4.24) in (4.23), and using $J^{e(3)} = J$, we obtain

$$\mathbf{T}^{(3)} = J^{-1}(2G^{(3)}\mathbf{E}_{\mathrm{H0}}^{e(3)} + K\,(\mathrm{tr}\mathbf{E}_{\mathrm{H}}^{e(3)})\mathbf{1}), \tag{4.25}$$

in which $\mathbf{E}_{\mathrm{H}}^{e(3)}$ is the spatial Hencky strain.

The evolution equation for $\mathbf{F}^{v(3)}$ is

$$\dot{\mathbf{F}}^{p(3)} = \mathbf{D}^{v(3)}\mathbf{F}^{v(3)}, \quad \mathbf{F}^{v(3)}(\mathbf{X}, 0) = \mathbf{1}, \tag{4.26}$$

with the viscous stretching given by

$$\mathbf{D}^{v(3)} = \dot{\bar{\gamma}}^{v(3)}\left(\frac{\mathbf{M}_0^{e(3)}}{2\bar{\tau}^{(3)}}\right), \tag{4.27}$$

where

$$\bar{\tau}^{(3)} \stackrel{\mathrm{def}}{=} \frac{1}{\sqrt{2}}|\mathbf{M}_0^{e(3)}| \tag{4.28}$$

defines an *equivalent shear stress* for viscous flow, with

$$\dot{\bar{\gamma}}^{v(3)} = f^{(3)}(\bar{\tau}^{(3)}, \mathbf{C}^{e(3)}, s^{(3)}, \vec{\xi}) \geq 0, \tag{4.29}$$

an *equivalent viscous shear strain rate*.

**The internal variable** $\xi^{(3)}$: As stated earlier, to account for the complex Mullins-type effect and the rate-sensitive response of a double-network hydrogel, the micromechanisms 2 and 3 are taken to *interact*. We account for such interactions by introducing a parameter

$$\varphi \in [0, 1],$$

which represents a fraction of the extent of the damage in ionically-crosslinked network, as measured by $\bar{\lambda}_{\max}$, and take $\xi^{(3)}$ to be given by

$$\xi^{(3)} \stackrel{\mathrm{def}}{=} \varphi\bar{\lambda}_{\max}. \tag{4.30}$$

This variable is in turn taken to affect the elasticity and the viscosity of the micromechanism $\alpha = 3$. As $\xi^{(3)}$ increases or decreases, the shear modulus, $G^{(3)}$, and the viscous flow resistance in shear, $s^{(3)}$, will be taken to increase or decrease. The evolution of $\varphi$ depends on the level $\bar{\lambda}$, and whether $\bar{\lambda}$ is increasing or decreasing, as discussed below:

(i) If $\bar{\lambda} = \bar{\lambda}_{\max}$ and $\dot{\bar{\lambda}} > 0$, a state we call "loading", then $\varphi$ is taken to evolve according to

$$\dot{\varphi} = A(1 - \varphi)\dot{\bar{\lambda}}, \tag{4.31}$$

with $A > 0$ a constant. That is, under continued loading $\varphi$ approaches unity, at a rate determined by $A(1 - \varphi)$, as the effective stretch $\bar{\lambda}$ increases.

(ii) If $\bar{\lambda} = \bar{\lambda}_{\max}$ and $\dot{\bar{\lambda}} < 0$, a state we call "unloading", then $\varphi$ is taken to evolve according to

$$\dot{\varphi} = A\,\varphi\dot{\bar{\lambda}}, \tag{4.32}$$

so that $\dot{\varphi}$ is negative. Thus, under continued unloading, $\varphi \to 0$ as the effective stretch $\bar{\lambda}$ decreases.

(iii) If $\bar{\lambda} < \bar{\lambda}_{\max}$ and $\dot{\bar{\lambda}} > 0$, a state we call "reloading", then $\varphi$ is taken to evolve in manner similar to (4.31) but with the factor $(1 - \varphi)$ replaced by $(\pi(\bar{\lambda}, \bar{\lambda}_{\max}) - \varphi)$, that is

$$\dot{\varphi} = A(\pi(\bar{\lambda}, \bar{\lambda}_{\max}) - \varphi)\dot{\bar{\lambda}}, \tag{4.33}$$

where $\pi(\bar{\lambda}, \bar{\lambda}_{\max})$ is a function of $\bar{\lambda}$ and $\bar{\lambda}_{\max}$, with values in the range $\pi(\bar{\lambda}, \bar{\lambda}_{\max}) \in [0, 1]$. The function $\pi(\bar{\lambda}, \bar{\lambda}_{\max})$ is presumed to be a monotonically increasing function of $\bar{\lambda}$ until $\bar{\lambda}$ reaches the current value of $\bar{\lambda}_{\max}$, at which point the evolution equation of $\varphi$ switches to case (4.31) discussed above. A particular form for $\pi(\bar{\lambda}, \bar{\lambda}_{\max})$, which satisfies the requirement above is

$$\pi(\bar{\lambda}, \bar{\lambda}_{\max}) = \left(\frac{\bar{\lambda} - 1}{\bar{\lambda}_{\max} - 1}\right)^2; \tag{4.34}$$

we adopt it here.

To summarize, we take $\xi^{(3)} = \varphi\bar{\lambda}_{\max}$, with the fraction $\varphi \in [0, 1]$ assumed to evolve according to

$$\dot{\varphi} = \begin{cases} A(1-\varphi)\dot{\bar{\lambda}} & \text{if } \bar{\lambda} = \bar{\lambda}_{\max} \text{ and } \dot{\bar{\lambda}} > 0, \\ A\varphi\dot{\bar{\lambda}} & \text{if } \bar{\lambda} \leq \bar{\lambda}_{\max} \text{ and } \dot{\bar{\lambda}} < 0, \\ A\left[\left(\dfrac{\bar{\lambda}-1}{\bar{\lambda}_{\max}-1}\right)^2 - \varphi\right]\dot{\bar{\lambda}} & \text{if } \bar{\lambda} < \bar{\lambda}_{\max} \text{ and } \dot{\bar{\lambda}} > 0, \end{cases}$$

(4.35)

with $A > 0$ a material parameter.

We assume that the bulk modulus $K$ is large relative to $G^{(3)}$, and essentially unaffected by the internal variable $\xi^{(3)} = \varphi\bar{\lambda}_{\max}$, while the shear modulus $G^{(3)}$ evolves according to

$$G^{(3)} = G_0^{(3)} + H_g(\varphi\bar{\lambda}_{\max})^r,$$

(4.36)

with $\{G_0^{(3)}, H_g, r\}$ all positive-valued parameters, so that $G^{(3)}$ increases or decreases as $\xi^{(3)} = \varphi\bar{\lambda}_{\max}$ increases or decreases.

Further the equivalent viscous shear strain rate in (4.29) is taken in a simple power law form

$$\dot{\bar{\gamma}}^{v(3)} = \dot{\gamma}_0\left(\frac{\bar{\tau}^{(3)}}{s^{(3)}}\right)^{1/m},$$

(4.37)

with $\dot{\gamma}_0$ a reference strain rate and $m$ a strain-rate sensitivity parameter, and where

$$s^{(3)} = s_0 + H_s(\varphi\bar{\lambda}_{\max})^n,$$

(4.38)

with $\{s_0, H_s, n\}$ all positive-valued parameters, so that $s^{(3)}$ increases or decreases as $\xi^{(3)} = \varphi\bar{\lambda}_{\max}$ increases or decreases.

Thus, the set of material parameters chosen to phenomenologically describe the intermolecular elastic-viscous response in our theory are

$$\{K, G_0^{(3)}, H_g, r, \dot{\gamma}_0, m, s_0, H_s, n, A\}.$$

(4.39)

## 5. Estimation of the material parameters in the theory

Using the information for sample preparation given in Section 2, and assuming that all solutions used in sample preparation have the same molar volume, we estimate the volume fractions as

$$\chi^{\text{solv}} = 0.877; \quad \chi^{(1)} = 0.103; \quad \chi^{(2)} = \chi^{(3)} = 0.010.$$

(5.1)

Idealizing the DN hydrogel to be completely *incompressible*, $J=1$, for simple extension in the $\mathbf{e}_2$ direction with respect to a recantangular Cartesian coordinate system with coordinate directions ($\mathbf{e}_1$, $\mathbf{e}_2$, $\mathbf{e}_3$), the matrices of the deformation gradient $\mathbf{F}$ and the Cauchy-Green tensors $\mathbf{C}$ and $\mathbf{B}$ are given by

$$\mathbf{F} = \mathbf{U} = \mathbf{V} = \begin{bmatrix} 1/\lambda^{1/2} & 0 & 0 \\ 0 & \lambda & 0 \\ 0 & 0 & 1/\lambda^{1/2} \end{bmatrix}, \quad \mathbf{C} = \mathbf{B} = \begin{bmatrix} 1/\lambda & 0 & 0 \\ 0 & \lambda^2 & 0 \\ 0 & 0 & 1/\lambda \end{bmatrix}.$$

(5.2)

### 5.1. Elasticity of the micromechanism $\alpha = 1$

Since the rotation in in simple extension is unity, $\mathbf{R} = \mathbf{1}$, the principal values $S_i^{(1)}$ of the contribution to the Piola stress $\mathbf{T}_R$ from micromechanism $\alpha = 1$ (under the assumption of complete incompressibility) are

$$S_i^{(1)} = G^{(1)}\lambda_i - p\lambda_i^{-1}, \quad \text{with} \quad G^{(1)} \overset{\text{def}}{=} C^{(1)}\left(1 - \frac{I_1 - 3}{I_m^{(1)}}\right)^{-1},$$

(5.3)

and $p$ an arbitrary pressure. Thus, for simple extension characterized by (5.2),

$$0 = S_1^{(1)} = S_3^{(1)} = G^{(1)}/\lambda^{1/2} - p\lambda^{1/2}, \quad S^{(1)} \equiv S_2^{(1)} = G^{(1)}\lambda - p\lambda^{-1}.$$

(5.4)

Eq. (5.4)$_1$ gives $p = G^{(1)}\lambda^{-1}$, substitution of which in (5.4)$_2$ gives the Piola stress $S^{(1)}$ in the $\mathbf{e}_2$-direction from the first micromechanism as

$$S^{(1)} = G^{(1)}(\lambda - \lambda^{-2}) \quad \text{with} \quad G^{(1)} \overset{\text{def}}{=} C^{(1)}\left(1 - \frac{I_1 - 3}{I_m^{(1)}}\right)^{-1},$$

(5.5)

where $I_1 = \lambda^2 + 2\lambda^{-1}$. The material parameters $C^{(1)}$ and $I_m^{(1)}$ in the generalized shear modulus $G^{(1)}$ were estimated by fitting the data from Fig. 3(a) for the long-chain network. The fit displayed in Fig. 7, was obtained with

$$C^{(1)} = 19.71 \text{ kPa}, \quad I_m^{(1)} = 330.$$

(5.6)

### 5.2. Elasticity with Mullins-type effect of micromechanism $\alpha = 2$

As in the previous subsection the Piola stress $S^{(2)}$ in the $\mathbf{e}_2$-direction from the second micromechanism which represents the
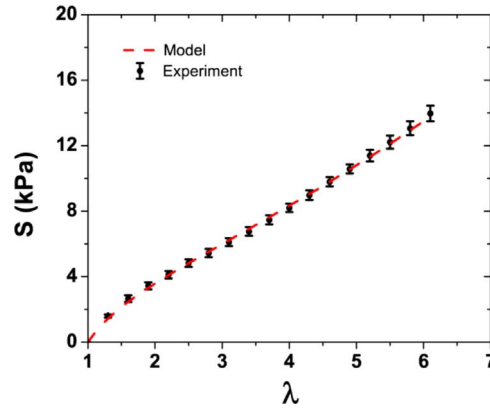
**Fig. 7.** Micromechanism $\alpha = 1$: comparison of the fit of the model shown as a dashed line, against experimental data shown as points with error bars.

elasticity together with a Mullins-type effect from the short-chain network, is given by

$$S^{(2)} = G^{(2)}(\lambda - \lambda^{-2}) \quad \text{with} \quad G^{(2)} \stackrel{\text{def}}{=} C^{(2)}\left(1 - \frac{I_1 - 3}{I_m^{(2)}}\right)^{-1},$$

(5.7)

where $I_1 = \lambda^2 + 2\lambda^{-1}$. Here $C^{(2)}$ and $I_m^{(2)}$ are two material functions which evolve according to Eqs. (4.13) and (4.15) to account for the Mullins-type effect. Thus, we need to estimate four parameters $\{C_0^{(2)}, I_{m,0}^{(2)}, p, q\}$. These material parameters were estimated by fitting the data in Fig. 5(d) for the short-chain network. The fit displayed in Fig. 8 was obtained with

$$C_0^{(2)} = 840 \text{ kPa}, \quad I_{m,0}^{(2)} = 4.3, \quad p = 0.196 \quad \text{and} \quad q = 2.$$

(5.8)

### 5.3. Viscoelastic response from micromechanism $\alpha = 3$

Here, with

$$\mathbf{F} = \begin{bmatrix} \lambda^{-1/2} & 0 & 0 \\ 0 & \lambda & 0 \\ 0 & 0 & \lambda^{-1/2} \end{bmatrix},$$

(5.9)

for simple tension, the matrices of components of $\mathbf{F}^{e(3)}$, $\mathbf{F}^{v(3)}$, and $\mathbf{D}^{v(3)}$ for an isotropic material are also diagonal,

$$\mathbf{F}^{e(3)} = \begin{bmatrix} \lambda_1^e & 0 & 0 \\ 0 & \lambda_2^e & 0 \\ 0 & 0 & \lambda_3^e \end{bmatrix}; \quad \mathbf{F}^{v(3)} = \begin{bmatrix} \lambda_1^v & 0 & 0 \\ 0 & \lambda_2^v & 0 \\ 0 & 0 & \lambda_3^v \end{bmatrix}; \quad \mathbf{D}^{v(3)} = \begin{bmatrix} d_1^v & 0 & 0 \\ 0 & d_2^v & 0 \\ 0 & 0 & d_3^v \end{bmatrix}.$$

(5.10)

From the kinematical relations we obtain

$$-\frac{1}{2}\overline{\ln \lambda} = \overline{\ln \lambda_1^e} + d_1^v, \quad \overline{\ln \lambda} = \overline{\ln \lambda_2^e} + d_2^v, \quad -\frac{1}{2}\overline{\ln \lambda} = \overline{\ln \lambda_3^e} + d_3^v,$$

(5.11)

and the deviatoric Mandel stress in the branch $\alpha = 3$ then has the form
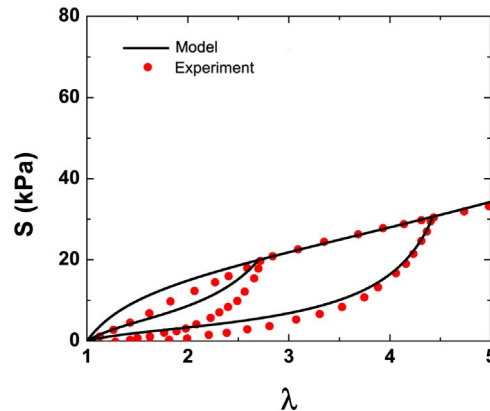


**Fig. 8.** Micromechanism $\alpha = 2$: comparison of the fit of the model shown as a solid line, against experimental data shown as points.
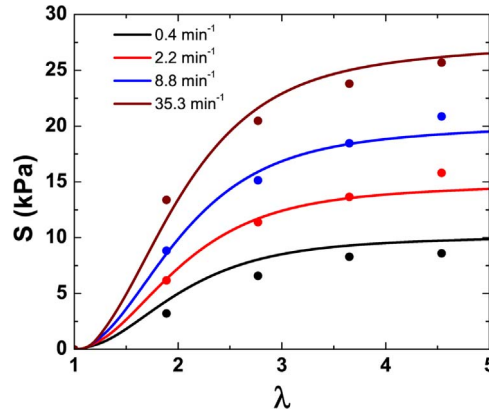
**Fig. 9.** The rate-dependent response of the DN hydrogel at different stretch rates during the monitonic loading. The filled dots represent the experimental data, while the solid lines are the model fits.

$$
\mathbf{M}_0^{e\,(3)} = 2G^{(3)}
\begin{bmatrix}
\ln \lambda_1^e - \frac{1}{3}\ln(\lambda_1^e \lambda_2^e \lambda_3^e) & 0 & 0 \\
0 & \ln \lambda_2^e - \frac{1}{3}\ln(\lambda_1^e \lambda_2^e \lambda_3^e) & 0 \\
0 & 0 & \ln \lambda_3^e - \frac{1}{3}\ln(\lambda_1^e \lambda_2^e \lambda_3^e)
\end{bmatrix},
$$
$$(5.12)$$

and correspondily the viscous stretching is

$$
\mathbf{D}^{v\,(3)} = \dot{\bar{\gamma}}^{v\,(3)}\left(\frac{\mathbf{M}_0^{e\,(3)}}{2\bar{\tau}^{(3)}}\right) = \dot{\gamma}_0 \left(\frac{\bar{\tau}^{(3)}}{s^{(3)}}\right)^{1/m}\left(\frac{\mathbf{M}_0^{e\,(3)}}{2\bar{\tau}^{(3)}}\right),
$$
$$(5.13)$$

with the elastic shear modulus $G^{(3)}$ and the shear resistance $s^{(3)}$ evolving according to Eqs. (4.30) and (4.38). The material paremeters for the viscoelastic response from branch $\alpha = 3$ (for an incompressible material) are $\{G_0^{(3)}, H_g, r, \dot{\gamma}_0, m, s_0, H_s, n, A\}$. These material parameters were estimated by fitting the data in Figs. 4(c), (d) and (b). The fits shown in Fig. 9 and Fig. 10 were obtained using[5]

$$
G_0^{(3)} = 20 \text{ kPa}, \quad H_g = 7048 \text{ kPa}, \quad r = 1.3, \quad \dot{\gamma}_0 = 1/\text{s}, \quad m = 0.22, \, s_0 = 20 \text{ kPa}, \quad H_s = 2588 \text{ kPa}, \quad n = 1.34, \quad A = 3. \quad (5.14)
$$

Fig. 9 shows the rate-dependent contribution during the monotonic loading at different stretch rates. The filled dots represent the experimental data, while the solid lines are the model fits. Our model captures the major features of the rate-dependent response of the material.

Fig. 10 displays the stress-relaxation response of the material. Specifically, Fig. 10(a) shows the stress-relaxation behavior at different stretch levels for a test conducted at a stretch rate of 8.8/min. In accord with the experimental data in Fig. 4(c), the model shows a weak stretch-dependence of the relaxation behavior. Fig. 10(b) shows the stress-relaxation behavior at different stretch rates. Our model captures the major features of the complex stress-relaxation response of the material.
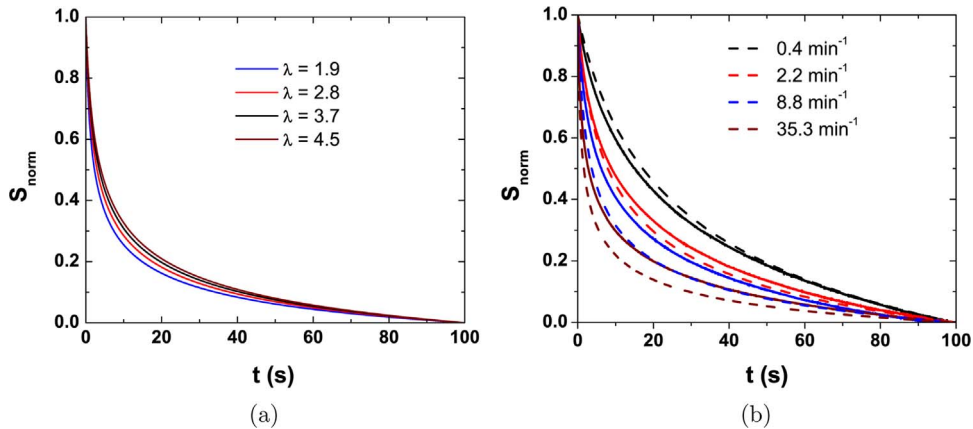


**Fig. 10.** Stress-relaxation response: (a) At different stretch levels for a test conducted at a nominal stretch rate of 8.8/min — a weak stretch-dependence (experimental data is not shown here). (b) At different stretch rates — a strong stretch-rate dependence. The solid lines represent the experimental data, while the dashed lines are the model fits.
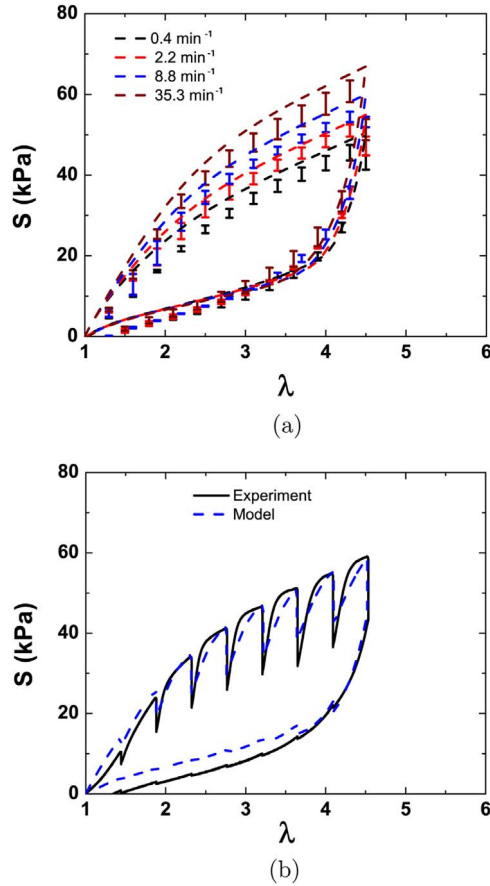
**Fig. 11.** Comparison between experiments and model for: (a) Cyclic loading without holding to a stretch 4.5 at various stretch rates. The dashed lines represent the results from the model. For clarity the corresponding experimental results are shown only as error bars so as not to crowd the figure. (b) Cyclic loading with holding at a stretch rate 8.8/min; the dashed line represents the result from the model, and the solid line the corresponding experimental result.

### 5.4. Overall response

The overall mechanical response predicted by our model in simple extension experiments is shown in Fig. 11. Specifically, Fig. 11(a) shows the predictions of model for stretching without holding at four different stretch rates.[6] While Fig. 11(b) shows the cyclic loading response at a nominal stretch rate 8.8/min, with intermittent holding. Overall, our model captures all the major features of the large deformation viscoelastic response of the DN hydrogel with reasonable accuracy. Recall, that in our model we have neglected the small rate-sensitivity of the unloading response, as well the small permanent set exhibited by the material.

The considerations so far have been to calibrate the material parameters of the theory from specimens deformed in simple extension. In the next section we test the response of the constitutive model in the very different mode of *simple shear*.

## 6. Simple shear

We have conducted an approximate "simple-shear" experiment on a specially-prepared double-shear specimen of the hydrogel; cf. Fig. 12 for a schematic of the experiment. The two gage sections of our double-shear specimen each had a width $W = 40$ mm and a height $H = 10$ mm. The thickness of the sample through the plane of the paper was $t = 6.375$ mm.

Fig. 13 shows two snapshots from the experiment: Fig. 13(a) shows the reference double-shear geometry, and Fig. 13(b) shows the deformed geometry after a large amount of shear. Note that this experimental geometry does not result in precise homogeneous simple shearing of the two gage sections, but only approximates such an ideal experiment.

In order to calculate a nominal shear-stress versus shear strain curve, the relevant cross-sectional area is $A = W \times t$, and the nominal shear stress is $S = F/A$, where $F$ is the force measured by the load cell of the testing machine. The nominal shear strain is $\gamma = d/H$, with $d$ is the imposed displacement of the crosshead in the horizontal direction. The nominal shear strain rate in our

---

[5] Since $\dot{\gamma}_0$ and $s^{(3)}$ cannot be fit separately, we have chosen a refrence shear rate of $\dot{\gamma}_0 = 1/s$.

[6] The numerically calculated stress-stretch results in Fig. 11(a) are slightly higher than the data shown as error bars for each stretch rate. We attribute this variability to the variability in the initial state of the double-network gel specimens — a variability which is difficult to control.
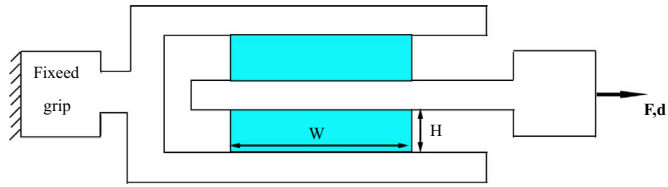
**Fig. 12.** Schematic of the double-shear experiment.
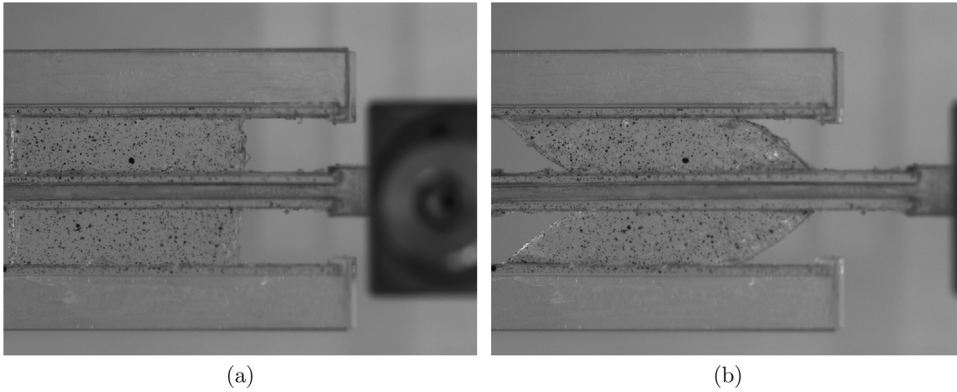


**Fig. 13.** Double-shear experiment (a) reference configuration; (b) deformed configuration.

experiment was $\dot{\gamma} = 0.1/s$, and also at each shear strain of $\gamma = 0.5n$, where $n$ is an integer, the sample was held for $25s$ in order to measure its stress-relaxation response.

In order to model the inhomogeneous deformation in this experiment, we implemented our constitutive model as a UMAT in ABAQUS/Standard (2014), and used this capability to conduct a simulation of the approximate simple shear experiment described above. Fig. 14(a) shows the finite element mesh,[7] and Fig. 14(b) shows the deformed mesh at a nominal shear strain of $\gamma = 1.5$, together with contours of the maximum effective stretch $\bar{\lambda}_{max}$.

Fig. 15 shows the experimentally-measured nominal shear stress versus nominal shear strain curve from the double-shear experiment (with intermittent hold during loading) as the solid line. The numerically calculated result is shown as the dashed line; it matches the experimental measurement quite well.

Finally we show a comparison between the experimentally-measured shapes of the gage section of the double-shear specimen and the corresponding shapes predicted by the numerical simulation in Fig. 16, at nominal shear strains of $\gamma = 1.5$ and $\gamma = 3.0$. In these figures, the dashed lines represent the simulated geometry, while the solid lines represent the experimentally-measured profiles. There is very good agreement between the experimentally-measured profiles and the numerically predicted profiles.

## 7. Concluding remarks

- We have conducted a set of pedigreed experiments on a double-network hydrogel which consists of a covalently-crosslinked polyacrylamide network with long chains, and an ionically-crosslinked alginate network with short chains. This double-network hydrogels shows three major characteristic responses which are different from conventional hydrogels:
  - (i) a large Mullins-type effect which manifests itself in hysteresis during loading and unloading;
  - (ii) an asymmetric rate-sensitive response during loading and unloading; and
  - (iii) a stretch-independent but stretch-rate dependent stress-relaxation behavior.
- We have developed a new large deformation viscoelasticity model to represent the complex mechanical response of this hydrogel, and presented a methodology for estimating the material parameters which appear in a specialized of set constitutive equations for the theory.
- We have shown that with suitably calibrated material parameters, the constitutive model can reproduce — with reasonable
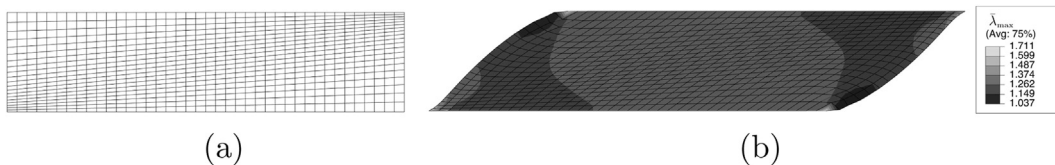


**Fig. 14.** Simulation of the simple shear experiment: (a) Undeformed mesh. (b) Deformed mesh at a nominal shear strain of $\gamma = 1.5$ The contours of the maximum effective stretch are also shown.
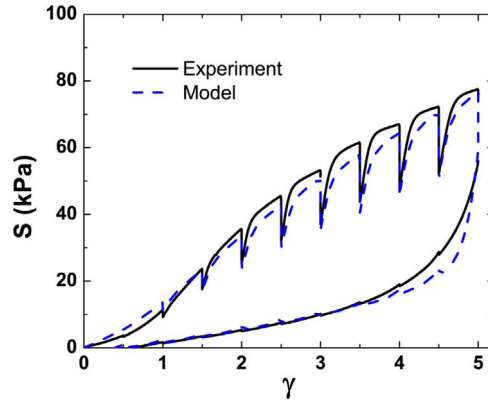
**Fig. 15.** Nominal shear stress versus nominal shear strain curve for double shear experiment with intermittent hold during loading. The experimental result is shown as the solid line, and the numerically calculated result is shown as the dashed line.
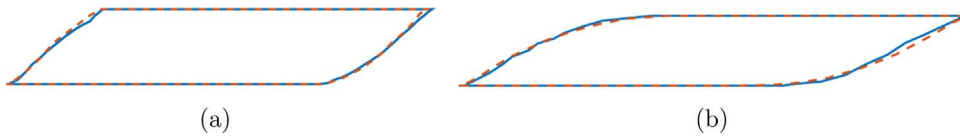


**Fig. 16.** Comparison of experimentally-measured and the numerically predicted shapes of the nominal "simple"-shear experiment, at shear strains of $\gamma = 1.5$ (a) and $\gamma = 3.0$ (b). The dashed lines represent the simulated geometry, while the solid lines represent the experimentally-measured profiles.

accuracy — the experimentally-measured response of the material in not only large simple extension experiments, but also large (nominal) simple shearing experiments.

- We believe that the constitutive theory presented in this paper should be useful to model the response of other similar hydrogels.[8]

As noted earlier, our model is restricted in the sense that in this study we limited our attention to conditions under which diffusion of the water in the hydrogel may be neglected. However, this condition does not hold in general, and what is needed is a coupled deformation-diffusion theory to model the complete response of this and other similar hydrogels. Also, the eventual fracture of such double-network hydrogels needs to be modeled. We leave such work to a future endeavor.

## Acknowledgments

## Appendix A. Detailed derivation of the theory

### A.1. Basic kinematics

Consider a macroscopically-homogeneous body B with the region of space it occupies in a fixed reference configuration, and denote by $\mathbf{X}$ an arbitrary material point of B. A motion of B is then a smooth one-to-one mapping $\mathbf{x} = \chi(\mathbf{X}, t)$ with deformation gradient, velocity, and velocity gradient given by

$$\mathbf{F} = \nabla \chi, \quad \mathbf{v} = \dot{\chi}, \quad \mathbf{L} = \text{grad } \mathbf{v} = \dot{\mathbf{F}} \mathbf{F}^{-1}. \tag{A.1}$$

We base our theory on a multiplicative decomposition of the deformation gradient

$$\mathbf{F} = \mathbf{F}^{e(\alpha)} \mathbf{F}^{v(\alpha)} \quad \alpha = 1, \ldots, M. \tag{A.2}$$

---

[7] This was a 3-D calculation using 800, C3D8H-ABAQUS elements in the plane of the paper, and one element through the thickness.

[8] As noted earlier in footnote 1, after we had submitted our paper for publication on November 18, 2016, a paper by Lu et al. (2017), which is on the same topic as our paper, has appeared online on November 22, 2016 in the ASME Journal of Applied Mechanics. Although the paper by these authors adresses the formulation of a constitutive model for soft materials which incorporates viscoelasticity and Mullins effect, as we do here, the details of the model in the paper by Lu et al. (2017) differ in many important respects from the one presented here. The differences are too numerous to discuss in detail, but we do note that these authors limit their attention to homogeneous deformations, formulate a model in principal stretch space, and fit their model to data in simple tension. Their model is not fully three-dimensional in nature, and it is unclear — and they have not shown — whether their model has validity for modes of deformation other than simple tension. Also, they have not implemented their model numerically in a finite element program, as we have reported in our paper.

We refer to $\mathbf{F}^{v(\alpha)}$ and $\mathbf{F}^{e(\alpha)}$ as the *viscous, and elastic distortions*, respectively.

As is standard, we assume that

$$J \overset{\text{def}}{=} \det \mathbf{F} > 0, \tag{A.3}$$

and hence, using (A.2),

$$J = J^{e(\alpha)} J^{v(\alpha)}. \tag{A.4}$$

We assume that

$$J^{e(\alpha)} \overset{\text{def}}{=} \det \mathbf{F}^{e(\alpha)} > 0, \qquad \text{and} \qquad J^{v(\alpha)} \overset{\text{def}}{=} \det \mathbf{F}^{v(\alpha)} > 0, \tag{A.5}$$

so that $\mathbf{F}^{e(\alpha)}$, $\mathbf{F}^{v(\alpha)}$ and $\mathbf{F}^s$ are invertible.

Thus, suppressing the argument $t$ for each micromechanism indexed by $\alpha$,

- $\mathbf{F}^{v(\alpha)}(\mathbf{X})$ represents the local inelastic distortion of the material at $\mathbf{X}$ due to a "viscous mechanism" such as the relative chain slippage of the long-chain polymer molecules. This local deformation carries the material into — and ultimately "pins" the material to — a *coherent structure* that resides in the *intermediate space* as represented by the range of $\mathbf{F}^{v(\alpha)}(\mathbf{X})$;
- $\mathbf{F}^{e(\alpha)}(\mathbf{X})$ represents the subsequent stretching and rotation of this coherent structure, and thereby represents the corresponding "mechanical" or "elastic" distortion, such as stretching of the long-chain polymer molecules and stretching of the intermolecular bonds.

### A.1.1. Polar decompositions

The right and left polar decomposition of $\mathbf{F}$ is given by

$$\mathbf{F} = \mathbf{R}\mathbf{U} = \mathbf{V}\mathbf{R}, \tag{A.6}$$

where $\mathbf{R}$ is a rotation (proper orthogonal tensor), while $\mathbf{U}$ and $\mathbf{V}$ are symmetric, positive-definite tensors with

$$\mathbf{U} = \sqrt{\mathbf{F}^{\mathsf{T}}\mathbf{F}}, \quad \mathbf{V} = \sqrt{\mathbf{F}\mathbf{F}^{\mathsf{T}}}. \tag{A.7}$$

Also, the right Cauchy-Green tensor is given by

$$\mathbf{C} = \mathbf{U}^2 = \mathbf{F}^{\mathsf{T}}\mathbf{F}, \quad \mathbf{B} = \mathbf{V}^2 = \mathbf{F}\mathbf{F}^{\mathsf{T}}. \tag{A.8}$$

Similarly, the right and left and polar decompositions of $\mathbf{F}^{e(\alpha)}$ are given by

$$\mathbf{F}^{e(\alpha)} = \mathbf{R}^{e(\alpha)}\mathbf{U}^{e(\alpha)} = \mathbf{V}^{e(\alpha)}\mathbf{R}^{e(\alpha)}, \tag{A.9}$$

where $\mathbf{R}^{e(\alpha)}$ is a rotation (proper orthogonal tensor), while $\mathbf{U}^{e(\alpha)}$ and $\mathbf{V}^{e(\alpha)}$ are symmetric, positive-definite tensors with

$$\mathbf{U}^{e(\alpha)} = \sqrt{\mathbf{F}^{e(\alpha)\mathsf{T}}\mathbf{F}^{e(\alpha)}}, \quad \mathbf{V}^{e(\alpha)} = \sqrt{\mathbf{F}^{e(\alpha)}\mathbf{F}^{e(\alpha)\mathsf{T}}}. \tag{A.10}$$

Also, the right and left elastic Cauchy-Green tensors are given by

$$\mathbf{C}^{e(\alpha)} = \mathbf{U}^{e(\alpha)2} = \mathbf{F}^{e(\alpha)\mathsf{T}}\mathbf{F}^{e(\alpha)}, \quad \mathbf{B}^{e(\alpha)} = \mathbf{V}^{e(\alpha)2} = \mathbf{F}^{e(\alpha)}\mathbf{F}^{e(\alpha)\mathsf{T}}. \tag{A.11}$$

### A.1.2. Velocity gradient

Next, by (A.1)$_3$ and (A.2),

$$\mathbf{L} = \mathbf{L}^{e(\alpha)} + \mathbf{F}^{e(\alpha)}\mathbf{L}^{v(\alpha)}\mathbf{F}^{e(\alpha)-1}, \tag{A.12}$$

with

$$\mathbf{L}^e = \dot{\mathbf{F}}^{e(\alpha)}\mathbf{F}^{e(\alpha)-1}, \quad \mathbf{L}^v = \dot{\mathbf{F}}^{p(\alpha)}\mathbf{F}^{v(\alpha)-1}. \tag{A.13}$$

As is standard, we define the total, elastic, viscous and swelling stretching and spin tensors through

$$\left.\begin{array}{ll} \mathbf{D} = \text{sym}\mathbf{L}, & \mathbf{W} = \text{skw}\mathbf{L}, \\ \mathbf{D}^{e(\alpha)} = \text{sym}\mathbf{L}^{e(\alpha)}, & \mathbf{W}^{e(\alpha)} = \text{skw}\mathbf{L}^{e(\alpha)}, \\ \mathbf{D}^{v(\alpha)} = \text{sym}\mathbf{L}^{v(\alpha)}, & \mathbf{W}^{v(\alpha)} = \text{skw}\mathbf{L}^{v(\alpha)}, \end{array}\right\} \tag{A.14}$$

so that $\mathbf{L} = \mathbf{D} + \mathbf{W}$, $\mathbf{L}^{e(\alpha)} = \mathbf{D}^{e(\alpha)} + \mathbf{W}^{e(\alpha)}$, and $\mathbf{L}^{v(\alpha)} = \mathbf{D}^{v(\alpha)} + \mathbf{W}^{v(\alpha)}$. Next, we make two basic kinematical assumptions concerning viscous flow:

(i) First, we make the standard assumption that viscous flow is incompressible, so that

$$J^{v(\alpha)} = \det \mathbf{F}^{v(\alpha)} = 1 \quad \text{and} \quad \text{tr}\,\mathbf{L}^{v(\alpha)} = \text{tr}\,\mathbf{D}^{v(\alpha)} = 0. \tag{A.15}$$

(ii) Hence, using (A.4), we note that

$$J^{e(\alpha)} = J \quad \text{for all } \alpha. \tag{A.16}$$

(iii)  Next, from the outset we constrain the theory by limiting our discussion to circumstances under which the material may be idealized as *isotropic*. For isotropic elastic-viscous theories utilizing the multiplicative decomposition of **F**, it is widely assumed that the viscous flow is *irrotational* (cf., e.g., Gurtin et al., 2010, Section 97) in the sense that

$$\mathbf{W}^{v(\alpha)} = \mathbf{0}. \tag{A.17}$$

Then, $\mathbf{L}^{v(\alpha)} \equiv \mathbf{D}^{v(\alpha)}$ and

$$\dot{\mathbf{F}}^{v(\alpha)} = \mathbf{D}^{v(\alpha)}\mathbf{F}^{v(\alpha)}. \tag{A.18}$$

Further, on account of (A.17), the relation (A.12) reduces to

$$\mathbf{L} = \mathbf{L}^{e(\alpha)} + \mathbf{F}^{e(\alpha)}\mathbf{D}^{v(\alpha)}\mathbf{F}^{v(\alpha)-1}. \tag{A.19}$$

Finally, using (A.1) and (A.3)$_2$ we may write (A.19), for future use, as

$$(\nabla\dot{\chi})\mathbf{F}^{-1} = \dot{\mathbf{F}}^{e(\alpha)}\mathbf{F}^{e(\alpha)-1} + \mathbf{F}^{e(\alpha)}\mathbf{D}^{v(\alpha)}\mathbf{F}^{e(\alpha)-1}. \tag{A.20}$$

### A.2. Frame-indifference

A change in frame, at each fixed time t, is a transformation — defined by a rotation $\mathbf{Q}(t)$ and a spatial point $\mathbf{y}(t)$ — which transforms spatial points **x** to spatial points:

$$\mathbf{x}^* = \mathcal{F}(\mathbf{x}), \quad = \mathbf{y}(t) + \mathbf{Q}(t)(\mathbf{x} - \mathbf{o}), \tag{A.21}$$

with **o** a fixed spatial origin. The function $\mathcal{F}$ thus represents a rigid mapping of the observed space into itself.

By (A.21) the transformation law for the motion $\mathbf{x} = \chi(\mathbf{X}, t)$ has the form

$$\chi^*(\mathbf{X}, t) = \mathbf{y}(t) + \mathbf{Q}(t)(\chi(\mathbf{X}, t) - \mathbf{o}). \tag{A.22}$$

Hence the deformation gradient **F** transforms according to

$$\mathbf{F}^* = \mathbf{QF}, \tag{A.23}$$

and

$$\mathbf{C} \text{ is invariant.} \tag{A.24}$$

- Since *frame changes only involve the observed space*, the reference space and the local intermediate spaces (which are the ranges of $\mathbf{F}^{v(\alpha)}(\mathbf{X})$) are independent of the choice of a change in frame.

Thus

$$\mathbf{F}^{v(\alpha)} \text{ are invariant under a change in frame.} \tag{A.25}$$

This observation, (A.2) and (A.23) yield the transformation law

$$\mathbf{F}^{v(\alpha)*} = \mathbf{QF}^{e(\alpha)}. \tag{A.26}$$

Also, using (A.13), (A.14) and (A.25),

$$\mathbf{D}^{v(\alpha)} \quad \text{is invariant,} \tag{A.27}$$

and, by (A.13)$_1$,

$$\mathbf{L}^{e(\alpha)*} = \mathbf{QL}^{e(\alpha)}\mathbf{Q}^{\mathsf{T}} + \dot{\mathbf{Q}}\mathbf{Q}^{\mathsf{T}},$$

and hence

$$\mathbf{D}^{e(\alpha)*} = \mathbf{QD}^{e(\alpha)}\mathbf{Q}^{\mathsf{T}}, \quad \mathbf{W}^{e(\alpha)*} = \mathbf{QW}^{e(\alpha)}\mathbf{Q}^{\mathsf{T}} + \dot{\mathbf{Q}}\mathbf{Q}^{\mathsf{T}}. \tag{A.28}$$

Further, by (A.9),

$$\mathbf{QF}^{e(\alpha)} = \mathbf{QR}^{e(\alpha)}\mathbf{U}^{e(\alpha)} = \mathbf{QV}^{e(\alpha)}\mathbf{Q}^{\mathsf{T}}\mathbf{QR}^{e(\alpha)},$$

and we may conclude from the uniqueness of the polar decomposition that

$$\mathbf{R}^{e(\alpha)*} = \mathbf{QR}^{e(\alpha)}, \quad \mathbf{V}^{e(\alpha)*} = \mathbf{QV}^{e(\alpha)}\mathbf{Q}^{\mathsf{T}}, \quad \mathbf{U}^{e(\alpha)} \text{ are invariant.} \tag{A.29}$$

In addition, on account of the definition (A.11) of $\mathbf{C}^{e(\alpha)}$ and (A.26),

$\mathbf{C}^{e(\alpha)}$ are also invariant. (A.30)

### A.3. Principle of virtual power. Balance of forces

The power expended on a part P by material or bodies exterior to P results from a *macroscopic surface traction* $\mathbf{t}_R(\mathbf{n}_R)$, measured per unit area in the reference body, and a *macroscopic body force* $\mathbf{b}_R$, measured per unit volume in the reference body, each of whose working accompanies the macroscopic motion of the body. The body force $\mathbf{b}_R$ is assumed to include inertial body force,

$$\mathbf{b}_R = \mathbf{b}_{0R} - \rho_R \ddot{\boldsymbol{\chi}}, \tag{A.31}$$

where $\mathbf{b}_{0R}$ is the conventional body force. We therefore write the *external power* as

$$\mathcal{W}_{\text{ext}}(P) = \int_{\partial P} \mathbf{t}_R(\mathbf{n}_R) \cdot \dot{\boldsymbol{\chi}} \; da_R + \int_P \mathbf{b}_R \cdot \dot{\boldsymbol{\chi}} \, dv_R. \tag{A.32}$$

Here, $\mathbf{t}_R(\mathbf{n}_R)$ and $\mathbf{b}_R$ are defined over the body for all time.

Next, we assume that power is expended internally by *elastic stresses* $\mathbf{S}^{e(\alpha)}$ power-conjugate to $\dot{\mathbf{F}}^{e(\alpha)}$, and *viscous stresses* $\mathbf{T}^{v(\alpha)}$ that expend power over the viscous stretchings $\mathbf{D}^{v(\alpha)}$, and we write the *internal power* as

$$\mathcal{W}_{\text{int}}(P) = \int_P \sum_\alpha \chi^{(\alpha)}(\mathbf{S}^{e(\alpha)}: \dot{\mathbf{F}}^{e(\alpha)} + \mathbf{T}^{v(\alpha)}: \mathbf{D}^{v(\alpha)}) dv_R, \tag{A.33}$$

Here, $\mathbf{S}^{e(\alpha)}$ and $\mathbf{T}^{v(\alpha)}$ are defined over the body for all time. We assume that the stresses $\mathbf{T}^{v(\alpha)}$ are symmetric and deviatoric, since $\mathbf{D}^{v(\alpha)}$ are symmetric and deviatoric. Also, each $\chi^{(\alpha)}$ is a constant positive-valued scalar fraction reflecting a contribution to the internal power from each micromechanism $\alpha$. The fractions $\chi^{(\alpha)}$ are presumed to satisfy the constraint

$$\sum_\alpha \chi^{(\alpha)} = 1 - \chi^{\text{solv}}, \tag{A.34}$$

where $\chi^{\text{solv}}$ is a constant volume fraction of solvent in the gel, *with the solvent assumed to have no contribution to the internal power expenditure.*

Assume that, at some arbitrarily chosen but *fixed time*, the fields $\boldsymbol{\chi}$, $\mathbf{F}$, $\mathbf{F}^{e(\alpha)}$, and $\mathbf{F}^{v(\alpha)}$, are known, and consider the fields $\dot{\boldsymbol{\chi}}$, $\dot{\mathbf{F}}^{e(\alpha)}$, and $\mathbf{D}^{v(\alpha)}$ as virtual velocities to be specified independently in a manner consistent with (A.20). That is, denoting the virtual fields by $\widetilde{\boldsymbol{\chi}}$, $\widetilde{\mathbf{F}}^{e(\alpha)}$, and $\widetilde{\mathbf{D}}^{v(\alpha)}$ to differentiate them from fields associated with the actual evolution of the body, we require that

$$(\nabla \dot{\boldsymbol{\chi}})\mathbf{F}^{-1} = \widetilde{\mathbf{F}}^{e(\alpha)}\mathbf{F}^{e(\alpha)-1} + \mathbf{F}^{e(\alpha)}\widetilde{\mathbf{D}}^{v(\alpha)}\mathbf{F}^{e(\alpha)-1}. \tag{A.35}$$

Further, we define a generalized virtual velocity to be a list

$$\mathcal{V} = (\widetilde{\boldsymbol{\chi}}, \widetilde{\mathbf{F}}^{e(\alpha)}, \widetilde{\mathbf{D}}^{v(\alpha)}),$$

consistent with (A.35).

**Remark.** We refer to a macroscopic virtual field $\mathcal{V}$ as *rigid* if it satisfies

$$(\nabla \widetilde{\boldsymbol{\chi}})\mathbf{F}^{-1} \equiv \widetilde{\mathbf{F}}\mathbf{F}^{-1} = \boldsymbol{\Omega} \Longrightarrow \widetilde{\mathbf{F}} = \boldsymbol{\Omega}\mathbf{F}, \tag{A.36}$$

with $\boldsymbol{\Omega}$ a spatially constant skew tensor, together with

$$\widetilde{\mathbf{F}}^{e(\alpha)} = \boldsymbol{\Omega}\mathbf{F}^{e(\alpha)}, \quad \text{and} \quad \widetilde{\mathbf{D}}^{v(\alpha)} = \mathbf{0}. \tag{A.37}$$

Writing

$$\left. \begin{array}{l} \mathcal{W}_{\text{ext}}(P, \mathcal{V}) = \int_{\partial P} \mathbf{t}_R(\mathbf{n}_R) \cdot \widetilde{\boldsymbol{\chi}} \; da_R + \int_P \mathbf{b}_R \cdot \widetilde{\boldsymbol{\chi}} \, dv_R, \\ \mathcal{W}_{\text{int}}(P, \mathcal{V}) = \int_P \sum_\alpha \chi^{(\alpha)}(\mathbf{S}^{e(\alpha)}: \widetilde{\mathbf{F}}^{e(\alpha)} + \mathbf{T}^{v(\alpha)}: \widetilde{\mathbf{D}}^{v(\alpha)}) \, dv_R, \end{array} \right\} \tag{A.38}$$

respectively, for the external and internal expenditures of virtual power, the *principle of virtual power* consists of two basic requirements:

(1) (Power Balance) Given any part P,

$$\mathcal{W}_{\text{ext}}(P, \mathcal{V}) = \mathcal{W}_{\text{int}}(P, \mathcal{V}) \quad \text{for all generalized virtual velocities } \mathcal{V}. \tag{A.39}$$

(2) (Rigid motion hypothesis) Given any part P and a rigid virtual velocity $\mathcal{V}$,

$$\mathcal{W}_{\text{int}}(P, \mathcal{V}) = 0 \quad \text{whenever } \mathcal{V} \text{ is a rigid macroscopic virtual velociy.} \tag{A.40}$$

Next, to deduce the consequences of the principle of virtual power. Assume that (A.35) and (A.36) are satisfied; in applying the virtual balance we are at liberty to choose any $\mathcal{V}$ consistent with the constraint (A.33).

### A.3.1. Macroscopic force and moment balances

Let $\widetilde{\mathbf{D}}^{v(\alpha)} = 0$ so that $\widetilde{\mathbf{F}}^{e(\alpha)} = (\nabla\widetilde{\chi})\mathbf{F}^{v(\alpha)-1}$. For this choice of $\mathcal{V}$, (A.35) yields

$$\int_{\partial P} \mathbf{t}_R(\mathbf{n}_R)\cdot\widetilde{\chi}\ da_R + \int_P \mathbf{b}_R\widetilde{\chi}\ dv_R = \int_P \sum_\alpha \chi^{(\alpha)}\mathbf{S}^{e(\alpha)}:\widetilde{\mathbf{F}}^{e(\alpha)}\ dv_R = \int_P \left(\sum_\alpha \chi^{(\alpha)}\mathbf{S}^{e(\alpha)}\mathbf{F}^{v(\alpha)-\top}\right):\nabla\widetilde{\chi}\ dv_R, \tag{A.41}$$

which, by defining

$$\mathbf{T}_R \overset{\text{def}}{=} \sum_\alpha \chi^{(\alpha)}\mathbf{S}^{e(\alpha)}\mathbf{F}^{v(\alpha)-\top}, \tag{A.42}$$

may be rewritten as

$$\int_{\partial P} \mathbf{t}_R(\mathbf{n}_R)\cdot\widetilde{\chi}\ da_R = \int_P (\mathbf{T}_R:\nabla\widetilde{\chi} - \mathbf{b}_R\cdot\widetilde{\chi})dv_R, \tag{A.43}$$

and using the divergence theorem we may conclude that

$$\int_{\partial P} (\mathbf{t}_R(\mathbf{n}_R) - \mathbf{T}_R\mathbf{n}_R)\cdot\widetilde{\chi}\ da_R + \int_P (\operatorname{Div}\mathbf{T}_R + \mathbf{b}_R)\cdot\widetilde{\chi}\ dv_R = 0.$$

Since this relation must hold for all P and all $\widetilde{\chi}$, standard variational arguments yield the traction condition

$$\mathbf{t}_R(\mathbf{n}_R) = \mathbf{T}_R\mathbf{n}_R, \tag{A.44}$$

and the local macroscopic force balance

$$\operatorname{Div}\mathbf{T}_R + \mathbf{b}_R = \mathbf{0}, \tag{A.45}$$

respectively.

Next, we deduce the consequences of requirement (V2) of the principle of virtual power. Using (A.36), (A.37), (A.42) and (A.38)$_2$, requirement (V2) of the principle of virtual power leads to the requirement that

$$0 = \int_P \sum_\alpha \chi^{(\alpha)}\mathbf{S}^{e(\alpha)}:(\boldsymbol{\Omega}\mathbf{F}^{e(\alpha)})\ dv_R, = \int_P \sum_\alpha \chi^{(\alpha)}(\mathbf{S}^{e(\alpha)}\mathbf{F}^{e(\alpha)\top}):\boldsymbol{\Omega}\ dv_R, = \int_P \left(\sum_\alpha \chi^{(\alpha)}(\mathbf{S}^{e(\alpha)}\mathbf{F}^{e(\alpha)\top}\mathbf{F}^{-\top})\mathbf{F}^\top\right):\boldsymbol{\Omega}\ dv_R,$$

$$= \int_P \left(\left(\sum_\alpha \chi^{(\alpha)}\mathbf{S}^{e(\alpha)}\mathbf{F}^{v(\alpha)-\top}\right)\mathbf{F}^\top\right):\boldsymbol{\Omega}\ dv_R, = \int_P (\mathbf{T}_R\mathbf{F}^\top):\boldsymbol{\Omega}\ dv_R. \tag{A.46}$$

Since P is arbitrary, we obtain that $(\mathbf{T}_R\mathbf{F}^\top):\boldsymbol{\Omega} = 0$ for all skew tensors $\Omega$, which implies that $\mathbf{T}_R\mathbf{F}^\top$ is *symmetric*:

$$\mathbf{T}_R\mathbf{F}^\top = \mathbf{F}\mathbf{T}_R^\top. \tag{A.47}$$

- Thus, the stress $\mathbf{T}_R$ represents the classical Piola stress, with (A.45) and (A.47) representing the local macroscopic force and moment balances in the reference body.

As is standard, the Piola stress $\mathbf{T}_R$ is related to the symmetric Cauchy stress $\mathbf{T}$ in the deformed body by

$$\mathbf{T}_R = J\,\mathbf{T}\mathbf{F}^{-\top}, \tag{A.48}$$

so that

$$\mathbf{T} = J^{-1}\mathbf{T}_R\mathbf{F}^\top. \tag{A.49}$$

Thus, using (A.42) and $\mathbf{F}^{e(\alpha)\top} = \mathbf{F}^{v(\alpha)-\top}\mathbf{F}^\top$,

$$\mathbf{T} = J^{-1}\left(\sum_\alpha \chi^{(\alpha)}\mathbf{S}^{e(\alpha)}\mathbf{F}^{v(\alpha)-\top}\right)\mathbf{F}^\top, = \sum_\alpha \chi^{(\alpha)}(J^{-1}\mathbf{S}^{e(\alpha)}\mathbf{F}^{e(\alpha)\top}), \tag{A.50}$$

and hence the Cauchy stress admits the additive decomposition

$$\mathbf{T} = \sum_\alpha \chi^{(\alpha)}\mathbf{T}^{(\alpha)}, \tag{A.51}$$

where

$$\mathbf{T}^{(\alpha)} \overset{\text{def}}{=} J^{-1}\mathbf{S}^{e(\alpha)}\mathbf{F}^{e(\alpha)\top}. \tag{A.52}$$

Since $\mathbf{T}$ is symmetric, we assume that each $\mathbf{T}^{(\alpha)}$ is *symmetric*.

As is standard, the macroscopic force balance (A.45) in the deformed body takes the form

$$\text{div } \mathbf{T} + \mathbf{b} = \mathbf{0}, \tag{A.53}$$

where

$$\mathbf{b} = J^{-1}(\mathbf{b}_{0\mathrm{R}} - \rho_0 \ddot{\boldsymbol{\chi}}) \equiv \mathbf{b}_0 - \rho \dot{\mathbf{v}}$$

is the body force per unit volume of the deformed body. Here, $\mathbf{b}_0$ is the body force per unit volume of the deformed body, $\rho$ the mass density in the deformed body, and $\dot{\mathbf{v}}$ the spatial description of the acceleration.

### A.3.2. Some new stress measures

It is convenient to introduce three new stress measures:

- The second Piola stress

  $$\mathbf{T}_{\mathrm{RR}} \overset{\text{def}}{=} \mathbf{F}^{-1}\mathbf{T}_{\mathrm{R}} = J\mathbf{F}^{-1}\mathbf{T}\mathbf{F}^{-\top}, \tag{A.54}$$

  which is symmetric.
- The elastic second Piola stresses

  $$\mathbf{T}^{e(\alpha)} \overset{\text{def}}{=} J^{e(\alpha)}\mathbf{F}^{e(\alpha)-1}\mathbf{T}^{(\alpha)}\mathbf{F}^{e(\alpha)-\top}, \tag{A.55}$$

  which is *symmetric* on account of the symmetry of the stress $\mathbf{T}^{(\alpha)}$.
- The Mandel stresses

  $$\mathbf{M}^{e(\alpha)} \overset{\text{def}}{=} \mathbf{C}^{e(\alpha)}\mathbf{T}^{e(\alpha)} = J^{e(\alpha)}\mathbf{F}^{e(\alpha)\top}\mathbf{T}^{(\alpha)}\mathbf{F}^{e(\alpha)-\top}, \tag{A.56}$$

  which in general are *not symmetric*.

From (A.52)$_1$ and (A.16),

$$\mathbf{S}^{e(\alpha)} = J^{e(\alpha)}\mathbf{T}^{(\alpha)}\mathbf{F}^{e(\alpha)-\top}, \tag{A.57}$$

which in general are *not symmetric*. Note that the stress measure $\mathbf{S}^{e(\alpha)}$ is the counterpart of the standard "first Piola stress" with respect to the intermediate space for each $\alpha$.

Hence, using the (definitions (A.55) and A.56), we find using (A.57) that

$$\mathbf{F}^{e(\alpha)-1}\mathbf{S}^{e(\alpha)} \quad \text{and} \quad \mathbf{F}^{e(\alpha)\top}\mathbf{S}^{e(\alpha)} = \mathbf{M}^{e(\alpha)}. \tag{A.58}$$

The standard transformation rules for the Piola stress $\mathbf{T}_{\mathrm{R}}$ and the Cauchy stress $\mathbf{T}$ under a change in frame are

$$\mathbf{T}_{\mathrm{R}}^* = \mathbf{Q}\mathbf{T}_{\mathrm{R}}, \quad \mathbf{T}^* = \mathbf{Q}\mathbf{T}\mathbf{Q}^\top, \tag{A.59}$$

while

$$\mathbf{T}_{\mathrm{RR}} \quad \text{is invariant.} \tag{A.60}$$

because of (A.59)$_2$

$$\mathbf{T}^{(\alpha)*} = \mathbf{Q}\mathbf{T}^{(\alpha)}\mathbf{Q}^\top. \tag{A.61}$$

Further, on account of the transformation rule (A.26) for $\mathbf{F}^{e(\alpha)}$, and the transformation rule (A.61), the elastic second Piola stresses and the Mandel stresses are invariant under a change in frame,

$$\mathbf{T}^{e(\alpha)*} = \mathbf{T}^{e(\alpha)} \quad \text{and} \quad \mathbf{M}^{e(\alpha)*} = \mathbf{M}^{e(\alpha)}. \tag{A.62}$$

### A.3.3. Microscopic force balances

To discuss the microscopic counterparts of macroscopic force balance, consider first a generalized virtual velocity with $\tilde{\boldsymbol{\chi}} = \mathbf{0}$, choose the virtual field $\widetilde{\mathbf{D}}^{\nu(\alpha)}$ arbitrarily, and let

$$\widetilde{\mathbf{F}}^{e(\alpha)} = -\mathbf{F}^{e(\alpha)}\widetilde{\mathbf{D}}^{\nu(\alpha)}.$$

Thus

$$\mathbf{S}^{e(\alpha)} : \widetilde{\mathbf{F}}^{e(\alpha)} = -\left((\mathbf{F}^{e(\alpha)\top}\mathbf{S}^{e(\alpha)}) : \widetilde{\mathbf{D}}^{\nu(\alpha)}\right) = -\left(\mathrm{sym}_0\mathbf{M}^{e(\alpha)} : \widetilde{\mathbf{D}}^{\nu(\alpha)}\right) \tag{A.63}$$

where we have used (A.58)$_2$ and the fact that $\widetilde{\mathbf{D}}^{\nu(\alpha)}$ is symmetric and deviatoric. The power balance (A.39) and (A.63) yield the *microscopic virtual-power relation*

$$0 = \int_{\mathrm{P}} \sum_\alpha \chi^{(\alpha)}\left(\mathbf{T}^{\nu(\alpha)} - \mathrm{sym}_0\mathbf{M}^{e(\alpha)}\right)\widetilde{\mathbf{D}}^{\nu(\alpha)} dv_{\mathrm{R}} \tag{A.64}$$

to be satisfied for all $\widetilde{\mathbf{D}}^{\nu(\alpha)}$ and all P. This yields the microscopic force balances

$$\mathrm{sym}_0\mathbf{M}^{e(\alpha)} = \mathbf{T}^{\nu(\alpha)}, \tag{A.65}$$

which characterizes the interaction between internal forces associated with the elastic and viscous response of the material.

Finally, using the traction condition (A.44), the actual external expenditure of power is

$$\mathcal{W}_{\mathrm{ext}}(\mathrm{P}) = \int_{\partial\mathrm{P}} (\mathbf{T}_{\mathrm{R}}\mathbf{n}_{\mathrm{R}})\cdot\dot{\chi} \; da_{\mathrm{R}} + \int_{\mathrm{P}} \mathbf{b}_{\mathrm{R}}\cdot\dot{\chi} \; dv_{\mathrm{R}}. \tag{A.66}$$

Next, differentiating (A.11)$_1$ results in the following expression for the rate of change of $\mathbf{C}$,

$$\dot{\mathbf{C}}^{e(\alpha)} = \mathbf{F}^{e(\alpha)\top}\dot{\mathbf{F}}^{e(\alpha)} + \dot{\mathbf{F}}^{e(\alpha)\top}\mathbf{F}^{e(\alpha)}.$$

Hence, since $\mathbf{T}^{e(\alpha)}$ is symmetric,

$$\mathbf{T}^{e(\alpha)}\colon \dot{\mathbf{C}}^{e(\alpha)} = 2\mathbf{T}^{e(\alpha)}\colon \mathbf{F}^{e(\alpha)\top}\dot{\mathbf{F}}^{e(\alpha)} = 2(\mathbf{F}^{e(\alpha)}\mathbf{T}^{e(\alpha)})\colon \dot{\mathbf{F}}^{e(\alpha)},$$

and upon using (A.58)$_1$, the stress power $\mathbf{S}^{e(\alpha)}\colon \dot{\mathbf{F}}^{e(\alpha)}$ may be alternatively written as

$$\mathbf{S}^{e(\alpha)}\colon \dot{\mathbf{F}}^{e(\alpha)} = \frac{1}{2}\mathbf{T}^{e(\alpha)}\colon \dot{\mathbf{C}}^{e(\alpha)}. \tag{A.67}$$

Thus the corresponding internal expenditure of power may be written as

$$\mathcal{W}_{\mathrm{int}}(\mathrm{P}) = \int_{\mathrm{P}} \sum_{\alpha} \chi^{(\alpha)}\left(\frac{1}{2}\mathbf{T}^{e(\alpha)}\colon \dot{\mathbf{C}}^{e(\alpha)} + \mathbf{T}^{\nu(\alpha)}\colon \mathbf{D}^{\nu(\alpha)}\right)dv_{\mathrm{R}}. \tag{A.68}$$

### A.4. Balance of energy. Entropy imbalance. Free energy imbalance

Our discussion of thermodynamics involves the following fields: $\varepsilon_{\mathrm{R}}$ the internal energy density per unit reference volume, $\eta_{\mathrm{R}}$ the entropy density per unit reference volume, $\mathbf{q}_{\mathrm{R}}$ the heat flux per unit reference area, $q_{\mathrm{R}}$ the external heat supply per unit reference volume, $\vartheta$ the absolute temperature ($\vartheta > 0$), For a material region P, we take the balance law for energy as (Gurtin et al., 2010)

$$\overline{\int_{\mathrm{P}} \varepsilon_{\mathrm{R}} \; dv_{\mathrm{R}}} = -\int_{\partial\mathrm{P}} \mathbf{q}_{\mathrm{R}}\cdot\mathbf{n}_{\mathrm{R}} \; da_{\mathrm{R}} + \int_{\mathrm{P}} q_{\mathrm{R}} \; dv_{\mathrm{R}} + \mathcal{W}_{\mathrm{ext}}(\mathrm{P}). \tag{A.69}$$

Also, the second law takes the form of an entropy imbalance

$$\overline{\int_{\mathrm{P}} \eta_{\mathrm{R}} \; dv_{\mathrm{R}}} \geq -\int_{\partial\mathrm{P}} \frac{\mathbf{q}_{\mathrm{R}}\cdot\mathbf{n}_{\mathrm{R}}}{\vartheta} \; da_{\mathrm{R}} + \int_{\mathrm{P}} \frac{q_{\mathrm{R}}}{\vartheta} \; dv_{\mathrm{R}}. \tag{A.70}$$

Assume now that *isothermal conditions* prevail, so that

$$\vartheta \equiv \text{constant},$$

and introduce the Helmholtz free energy per unit reference volume defined by

$$\psi_{\mathrm{R}} = \varepsilon_{\mathrm{R}} - \vartheta\eta_{\mathrm{R}}. \tag{A.71}$$

Then, upon multiplying the entropy imbalance (A.70) by $\vartheta$ and subtracting the result from the energy balance (A.69) yields the free energy imbalance

$$\overline{\int_{\mathrm{P}} \psi_{\mathrm{R}} \; dv_{\mathrm{R}}} \leq \mathcal{W}_{\mathrm{ext}}(\mathrm{P}). \tag{A.72}$$

We henceforth restrict attention to *isothermal processes* and for that reason base the theory on the free energy imbalance (A.72).

Thus, since $\mathcal{W}_{\mathrm{ext}}(\mathrm{P}) = \mathcal{W}_{\mathrm{int}}(\mathrm{P})$, upon recalling (A.68) and applying the divergence theorem to the term in (A.72) involving an integral over the boundary $\partial\mathrm{P}$ of P, we obtain

$$\int_{\mathrm{P}} \left(\dot{\psi}_{\mathrm{R}} - \sum_{\alpha} \chi^{(\alpha)}(1/2)\mathbf{T}^{e(\alpha)}\colon \dot{\mathbf{C}}^{e(\alpha)} - \sum_{\alpha} \chi^{(\alpha)}\mathbf{T}^{\nu(\alpha)}\colon \mathbf{D}^{\nu(\alpha)}\right)dv_{\mathrm{R}} \leq 0, \tag{A.73}$$

and using the fact that (A.73) must hold for all parts P, gives the local form of the free energy imbalance as

$$\dot{\psi}_{\mathrm{R}} - \sum_{\alpha} \chi^{(\alpha)}(1/2)\mathbf{T}^{e(\alpha)}\colon \dot{\mathbf{C}}^{e(\alpha)} - \sum_{\alpha} \chi^{(\alpha)}\mathbf{T}^{\nu(\alpha)}\colon \mathbf{D}^{\nu(\alpha)} \leq 0. \tag{A.74}$$

For later use we define the dissipation density $\mathcal{D} \geq 0$ per unit volume per unit time by

$$\mathcal{D} = \sum_{\alpha} \chi^{(\alpha)}(1/2)\mathbf{T}^{e(\alpha)}\colon \dot{\mathbf{C}}^{e(\alpha)} + \sum_{\alpha} \chi^{(\alpha)}\mathbf{T}^{\nu(\alpha)}\colon \mathbf{D}^{\nu(\alpha)} - \dot{\psi}_{\mathrm{R}} \geq 0. \tag{A.75}$$

Note that with the invariance properties discussed previously, all quantities in (A.74) and (A.75) are invariant under a change in frame.

### A.5. Constitutive theory

We limit our attention to situations under which the material may be idealized to be *isotropic*. Accordingly, all constitutive functions considered below are presumed to be isotropic in character.

#### A.5.1. Energetic constitutive equations

We introduce the notation

$$\vec{\mathbf{C}}^e = \{\mathbf{C}^{e(1)}, \ldots, \mathbf{C}^{e(M)}\},$$

to represent the set of all $\mathbf{C}^{e(\alpha)}$, and in order to account for the microstructural changes that alter the number of the ionic or covalent crosslinks in the material during deformation we introduce a list $M$ scalar internal variables $\xi^{(\alpha)}$, one for each micromechanism $\alpha$,

$$\vec{\xi} = \{\xi^{(1)}, \ldots, \xi^{(M)}\}.$$

Guided by the free energy imbalance (A.74) we first consider constitutive equations for the free energy $\psi_\mathrm{R}$ and the stresses $\mathbf{T}^{e(\alpha)}$ of the form

$$\left.\begin{aligned}
\psi_\mathrm{R} &= \chi^\mathrm{solv} \psi_\mathrm{R}^\mathrm{solv} + \sum_\alpha \chi^{(\alpha)} \psi_\mathrm{R}^{(\alpha)}(\mathbf{C}^{e(\alpha)}, \xi^{(\alpha)}), \\
\mathbf{T}^{e(\alpha)} &= \widehat{\mathbf{T}}^{e(\alpha)}(\mathbf{C}^{e(\alpha)}, \xi^{(\alpha)}).
\end{aligned}\right\} \tag{A.76}$$

Here, $\psi_\mathrm{R}^\mathrm{solv}$ is the contribution to free energy due to presence of the solvent, which we have presumed to be constant, and $\psi_\mathrm{R}^{(\alpha)}(\mathbf{C}^{e(\alpha)}, \xi^{(\alpha)})$ represent the mechanical contribution to the free energy from the different micromechanisms.

Substituting the constitutive equations (A.76) into the free-energy imbalance (A.74), we find that it may then be written as

$$\sum_\alpha \chi^{(\alpha)} \left[\frac{\partial \psi_\mathrm{R}^{(\alpha)}(\mathbf{C}^{e(\alpha)}, \xi^{(\alpha)})}{\partial \mathbf{C}^{e(\alpha)}} - \frac{1}{2}\widehat{\mathbf{T}}^{e(\alpha)}(\mathbf{C}^{e(\alpha)}, \xi^{(\alpha)})\right] : \dot{\mathbf{C}}^{e(\alpha)} + \sum_\alpha \chi^{(\alpha)} \frac{\partial \psi_\mathrm{R}^{(\alpha)}(\mathbf{C}^{e(\alpha)}, \xi^{(\alpha)})}{\partial \xi^{(\alpha)}} \dot{\xi}^{(\alpha)} - \sum_\alpha \chi^{(\alpha)} \mathbf{T}^{v(\alpha)} : \mathbf{D}^{v(\alpha)} \leq 0. \tag{A.77}$$

We assume that — constitutively — the stresses $\mathbf{T}^{v(\alpha)}$ are independent of $\dot{\mathbf{C}}^{e(\alpha)}$; thus, since these rates appear linearly in inequality (A.77), this inequality can hold for all values of $\dot{\mathbf{C}}^e$ only if the stressses $\mathbf{T}^{e(\alpha)}$ are given by the constitutive realtions

$$\mathbf{T}^{e(\alpha)} = 2\frac{\partial \psi_\mathrm{R}^{(\alpha)}(\mathbf{C}^{e(\alpha)}, \xi^{(\alpha)})}{\partial \mathbf{C}^{e(\alpha)}}, \tag{A.78}$$

and we are left with the following reduced dissipation inequality

$$\mathcal{D} = -\sum_\alpha \chi^{(\alpha)} \frac{\partial \psi_\mathrm{R}^{(\alpha)}(\mathbf{C}^{e(\alpha)}, \xi^{(\alpha)})}{\partial \xi^{(\alpha)}} \dot{\xi}^{(\alpha)} + \sum_\alpha \chi^{(\alpha)} \mathbf{T}^{v(\alpha)} : \mathbf{D}^{v(\alpha)} \geq 0. \tag{A.79}$$

To rule out trivial cases, we assume that the following *dissipation inequalities*

$$-\frac{\partial \psi_\mathrm{R}^{(\alpha)}(\mathbf{C}^{e(\alpha)}, \xi^{(\alpha)})}{\partial \xi^{(\alpha)}} \dot{\xi}^{(\alpha)} \geq 0, \quad \mathbf{T}^{v(\alpha)} : \mathbf{D}^{v(\alpha)} \geq 0, \tag{A.80}$$

must hold for for each $\alpha$. Dissipation is therefore characterized by the two inequalities above:

- the first, cf. (A.80)$_1$, represents the dissipation due to network alterations due to changes in $\xi^{(\alpha)}$; while
- the second, cf. (A.80)$_2$, represents the dissipation due to viscous flow.

#### A.5.2. Isotropic free energy

For isotropic materials the free energy functions $\psi_\mathrm{R}^{(\alpha)}(\mathbf{C}^{e(\alpha)}, \xi^{(\alpha)})$ are isotropic functions of their arguments. An immediate consequence is that these free energy functions have the representation

$$\psi_\mathrm{R}^{(\alpha)}(\mathbf{C}^{e(\alpha)}, \xi^{(\alpha)}) = \overline{\psi}_\mathrm{R}^{(\alpha)}(\mathcal{I}_{\mathbf{C}^{e(\alpha)}}, \xi^{(\alpha)}), \tag{A.81}$$

with

$$\mathcal{I}_{\mathbf{C}^{e(\alpha)}} = \left(I_1(\mathbf{C}^{e(\alpha)}), I_2(\mathbf{C}^{e(\alpha)}), I_3(\mathbf{C}^{e(\alpha)})\right)$$

the list of principal invariants of $\mathbf{C}^{e(\alpha)}$.

Thus, from (A.78)$_1$, it follows that

$$\mathbf{T}^{e(\alpha)} = 2\frac{\partial \psi_\mathrm{R}^{(\alpha)}(\mathcal{I}_{\mathbf{C}^{e(\alpha)}}, \xi^{(\alpha)})}{\partial \mathbf{C}^{e(\alpha)}}, \tag{A.82}$$

and that $\mathbf{T}^{e(\alpha)}$ is an *isotropic function of* $\mathbf{C}^{e(\alpha)}$. Hence, $\mathbf{T}^{e(\alpha)}$ and $\mathbf{C}^{e(\alpha)}$ commute,

$$\mathbf{C}^{e(\alpha)} \mathbf{T}^{e(\alpha)} = \mathbf{T}^{e(\alpha)} \mathbf{C}^{e(\alpha)}. \tag{A.83}$$

Then, since the Mandel stresses are defined by (cf. (A.56))

$$\mathbf{M}^{e(\alpha)} = \mathbf{C}^{e(\alpha)}\mathbf{T}^{e(\alpha)},$$

we find that *the Mandel stresses* $\mathbf{M}^{e(\alpha)}$ *is symmetric.*

Next, from (A.55) $\mathbf{T}^{(\alpha)} = J^{e(\alpha)-1}\mathbf{F}^{e(\alpha)}\mathbf{T}^{e(\alpha)}\mathbf{F}^{e(\alpha)\top}$, and hence using (A.82)

$$\mathbf{T}^{(\alpha)} = J^{e(\alpha)-1}\left(2\mathbf{F}^{e(\alpha)}\frac{\partial \psi_{\mathrm{R}}^{(\alpha)}(\mathcal{I}_{\mathbf{C}^{e(\alpha)}},\,\xi^{(\alpha)})}{\partial \mathbf{C}^{e(\alpha)}}\mathbf{F}^{e(\alpha)\top}\right). \tag{A.84}$$

Since $\mathbf{T} = \sum_{\alpha}\chi^{(\alpha)}\mathbf{T}^{(\alpha)}$ and $J^{e(\alpha)} = J$, we obtain

$$\mathbf{T} = J^{-1}\sum_{\alpha}\chi^{(\alpha)}\left(2\mathbf{F}^{e(\alpha)}\frac{\partial \psi_{\mathrm{R}}^{(\alpha)}(\mathcal{I}_{\mathbf{C}^{e(\alpha)}},\,\xi^{(\alpha)})}{\partial \mathbf{C}^{e(\alpha)}}\mathbf{F}^{e(\alpha)\top}\right). \tag{A.85}$$

Finally, on account of the symmetry of the Mandel stresses, the microforce balances (A.65) reduce to

$$\mathbf{M}_0^{e(\alpha)} = \mathbf{T}^{v(\alpha)}. \tag{A.86}$$

### A.5.3. Constitutive equations for $\mathbf{T}^{v(\alpha)}$. Hardening variables $\overrightarrow{s}$ and their evolution

To account for the major strain-hardening/softening characteristics of materials observed during viscous deformation, we introduce a set of **internal variables** which represent important aspects of the microstructural resistance to viscous flow.

- A list of $M$ scalar *internal state-variables*

$$\overrightarrow{s} = (s^{(1)},\,s^{(2)},...,s^{(M)}).$$

It is convenient to introduce the notation

$$\Lambda^{\alpha} = (\mathbf{C}^{e(\alpha)},\,s^{(\alpha)},\,\overrightarrow{\xi}). \tag{A.87}$$

Then, guided by inequality (A.80)$_2$, we take the stresses $\mathbf{T}^{v(\alpha)}$ to be given by constitutive equations of the form

$$\mathbf{T}^{v(\alpha)} = \mathbf{Y}^{v(\alpha)}(\mathbf{D}^{v(\alpha)},\,\Lambda^{(\alpha)}), \tag{A.88}$$

and presume that the internal variables $s^{(\alpha)}$ evolve according to

$$\dot{s}^{(\alpha)} = H^{(\alpha)}(\mathbf{D}^{v(\alpha)},\,\Lambda^{(\alpha)}). \tag{A.89}$$

### A.5.4. Flow rule

Upon using the constitutive relation for $\mathbf{T}^{v(\alpha)}$ above and the microforce balances (A.86), a central result of our theory is the **flow rule**,

$$\mathbf{M}_0^{e(\alpha)} = \mathbf{Y}^{v(\alpha)}(\mathbf{D}^{v(\alpha)},\,\Lambda^{(\alpha)}) \quad \text{for each } \alpha. \tag{A.90}$$

*Codirectionality hypothesis*

Let

$$\dot{\gamma}^{v(\alpha)} \overset{\text{def}}{=} \sqrt{2}\,|\mathbf{D}^{v(\alpha)}|, \tag{A.91}$$

denote a *equivalent viscous shear strain rate* for the $\alpha$th micromechanism. Then,

$$\mathbf{N}^{v(\alpha)} = \frac{\mathbf{D}^{v(\alpha)}}{|\mathbf{D}^{v(\alpha)}|} \quad \text{with} \quad \operatorname{tr}\mathbf{N}^{v(\alpha)} = 0, \quad \text{when} \quad \mathbf{D}^{v(\alpha)} \neq \mathbf{0}, \tag{A.92}$$

defines the **viscous flow direction** for the $\alpha$th micromechanism, so that

$$\mathbf{D}^{v(\alpha)} = \frac{1}{\sqrt{2}}\dot{\gamma}^{v(\alpha)}\mathbf{N}^{v(\alpha)}. \tag{A.93}$$

Then, the mechanical dissipation inequality (A.80)$_2$ requires that

$$\left(\frac{1}{\sqrt{2}}\mathbf{Y}^{v(\alpha)}\colon \mathbf{N}^{v(\alpha)}\right)\dot{\gamma}^{v(\alpha)} \geq 0 \tag{A.94}$$

Guided by this dissipation inequality, we henceforth adopt the **codirectionality hypothesis**, which asserts that

- each dissipative flow stress $\mathbf{Y}^{v(\alpha)}$ **is parallel to and points in the same direction as** $\mathbf{N}^{v(\alpha)}$:

$$\mathbf{Y}^{v(\alpha)}(\mathbf{D}^{v(\alpha)}, \Lambda^{(\alpha)}) = \sqrt{2}\ Y^{(\alpha)}(\dot{\bar{\gamma}}^{v(\alpha)}, \mathbf{N}^{v(\alpha)}, \Lambda^{(\alpha)})\mathbf{N}^{v(\alpha)}, \tag{A.95}$$

where

$$Y^{(\alpha)}(\dot{\bar{\gamma}}^{v(\alpha)}, \mathbf{N}^{v(\alpha)}, \Lambda^{(\alpha)}) = \frac{1}{\sqrt{2}}\mathbf{Y}^{v(\alpha)}(\mathbf{D}^{v(\alpha)}, \Lambda^{(\alpha)}) : \mathbf{N}^{v(\alpha)} \tag{A.96}$$

represents a scalar **shear flow strength** for the $\alpha$th micromechanism.

*Strong isotropy hypothesis*

We also assume that each scalar flow strength $Y^{(\alpha)}(\dot{\bar{\gamma}}^{v(\alpha)}, \mathbf{N}^{v(\alpha)}, \Lambda^{(\alpha)})$ and the hardening functions $H^{(\alpha)}(\dot{\bar{\gamma}}^{v(\alpha)}, \mathbf{N}^{v(\alpha)}, \Lambda^{(\alpha)})$ characterizing the evolution of the scalar internal variable $s^{(\alpha)}$ are **independent of the flow direction** $\mathbf{N}^{v(\alpha)}$, so that

$$Y^{(\alpha)}(\dot{\bar{\gamma}}^{v(\alpha)}, \Lambda^{(\alpha)}), \qquad H^{(\alpha)}(\dot{\bar{\gamma}}^{v(\alpha)}, \Lambda^{(\alpha)}).$$

Thus, using $\mathbf{Y}^{v(\alpha)} = \sqrt{2}\ Y^{(\alpha)}\mathbf{N}^{v(\alpha)}$, the flow rule (A.90) reduces to

$$\mathbf{M}_0^{e(\alpha)} = \sqrt{2}\ Y^{(\alpha)}(\dot{\bar{\gamma}}^{v(\alpha)}, \Lambda^{(\alpha)})\mathbf{N}^{v(\alpha)},$$

which immediately gives

$$\mathbf{N}^{v(\alpha)} = \frac{\mathbf{M}_0^e}{|\mathbf{M}_0^e|}, \tag{A.97}$$

and

$$\bar{\tau}^{(\alpha)} = Y^{(\alpha)}(\dot{\bar{\gamma}}^{v(\alpha)}, \Lambda^{(\alpha)}), \tag{A.98}$$

where we have introduced an **equivalent shear stress** $\bar{\tau}^{(\alpha)}$, defined by

$$\bar{\tau}^{(\alpha)} \overset{\text{def}}{=} \frac{1}{\sqrt{2}}|\mathbf{M}_0^{e(\alpha)}|. \tag{A.99}$$

- When $\bar{\tau}^{(\alpha)}$ and $\Lambda^{(\alpha)}$ are known, (A.98) serves as an implicit equation for the equivalent viscous shear strain rate rate $\dot{\bar{\gamma}}^{v(\alpha)}$ whenever it is non-zero.

  Note that from (A.94) and (A.96) and (A.98) that the viscous dissipation for each micromechanism is given by

$$Y^{(\alpha)}\dot{\bar{\gamma}}^{v(\alpha)} > 0 \quad \text{for} \quad \dot{\bar{\gamma}}^{v(\alpha)} > 0. \tag{A.100}$$

  We assume that

$$Y^{(\alpha)}(\dot{\bar{\gamma}}^{v(\alpha)}, \Lambda^{(\alpha)}) \text{ is a } \textbf{positive} - \textbf{valued strictly increasing function of } \dot{\bar{\gamma}}^{v(\alpha)}, \tag{A.101}$$

so

(i) that the dissipation inequality (A.100) is satisfied, and
(ii) that each fixed $\Lambda^{(\alpha)}$, the function $Y^{(\alpha)}(\dot{\bar{\gamma}}^{v(\alpha)}, \Lambda^{(\alpha)})$ is **invertible**.

Hence,

$$\dot{\bar{\gamma}}^{v(\alpha)} = f^{(\alpha)}(\bar{\tau}^{(\alpha)}, \Lambda^{(\alpha)}) \geq 0. \tag{A.102}$$

Thus, the evolution equation for each $\mathbf{F}^{v(\alpha)}$ is

$$\dot{\mathbf{F}}^{v(\alpha)} = \mathbf{D}^{v(\alpha)}\mathbf{F}^{v(\alpha)}, \quad \mathbf{F}^{v(\alpha)}(\mathbf{X}, 0) = \mathbf{1}, \tag{A.103}$$

with the viscous stretching given by

$$\mathbf{D}^{v(\alpha)} = \dot{\bar{\gamma}}^{v(\alpha)}\left(\frac{\mathbf{M}_0^{e(\alpha)}}{2\bar{\tau}^{(\alpha)}}\right), \tag{A.104}$$

and $\dot{\bar{\gamma}}^{v(\alpha)}$ given by (A.102).

# References

ABAQUS/Standard, 2014. SIMULIA, Providence, RI.

Ames, N.M., Srivastava, V., Chester, S.A., Anand, L., 2009. A thermo-mechanically coupled theory for large deformations of amorphous polymers. Part II: applications. Int. J. Plast. 25, 1495–1539.

Anand, L., 1979. On H. Hencky's approximate strain-energy function for moderate deformations. ASME J. Appl. Mech. 46, 78–82.

Anand, L., 1986. Moderate deformations in extension-torsion of incompressible isotropic elastic materials. J. Mech. Phys. Solids 34, 293–304.

Anand, L., Ames, N.M., Srivastava, V., Chester, S.A., 2009. A thermo-mechanically coupled theory for large deformations of amorphous polymers. Part I formulation. Int. J. Plast. 25, 1474–1494.

Arruda, E.M., Boyce, M.C., 1993. A three-dimensional constitutive model for the large stretch behavior of rubber elastic materials. J. Mech. Phys. Solids 41, 389–412.

Boyce, M.C., 1996. Direct comparison of the Gent and the Arruda-Boyce constitutive models of rubber elasticity. Rubber Chem. Technol. 69, 781–785.

Boyce, M.C., Socrate, S., Llana, P.G., 2000. Constitutive model for the finite deformation stress-strain behavior of poly(ethylene terephthalate) above the glass transition. Polymer 41, 2183–2201.

Chagnon, G., Verron, E., Marckmann, G., 2006. Development of new constitutive equations for the Mullins effect in rubber using the network alteration theory. Int. J. Solids Struct. 43, 6817–6831.

Cho, H., Rinaldi, R.G., Boyce, M.C., 2013. Constitutive modeling of the rate-dependent resilient and dissipative large deformation behavior of segmented copolymer polyurea. Soft Matter 9, 6319–6330.

Ducort, E., Chen, Y., Vulters, M., Sijbesma, R.P., Creton, C., 2014. Toughening elastomers with scarifical bonds and watching them break. Science 344, 186–189.

Gent, A.N., 1996. A new constitutive relation for rubber. Rubber Chem. Technol. 69, 59–61.

Gurtin, M.E., Fried, E., Anand, L., 2010. The Mechanics and Thermodynamics of Continua. Cambridge University Press, Cambridge.

Gong, J.P., Katsuyama, Y., Kurokawa, T., Osada, Y., 2003. Double-network hydrogels with extremely high mechanical strength. Adv. Mater. 15, 1155–1158.

Gong, J.P., 2010. Why are double network hydrogels so tough? Soft Matter 64, 2583–2590.

Gong, J.P., 2014. Materials both tough and soft. Science 344, 161–162.

Lu, T., Wang, J., Yang, R., Wang, T.J., 2017. A constitutive model for soft materials incorporating viscoelasticity and mullins effect. J. Appl. Mech. 84, 021010-1–021010-9.

Marckmann, G., Verron, E., Gornet, L., Chagnon, G., Charrier, P., Fort, P., 2002. A theory of network alteration for the Mullins effect. J. Mech. Phys. Solids 50, 2011–2028.

Mullins, L., 1969. Softening of rubber by deformation. Rubber Chem. Technol. 42, 339–362.

Srivastava, V., Chester, S.A., Ames, N.M., Anand, L., 2010a. A thermo-mechanically-coupled large-deformation theory for amorphous polymers in a temperature range which spans their glass transition. Int. J. Plast. 26, 1138–1182.

Srivastava, V., Chester, S.A., Anand, L., 2010b. Thermally actuated shape-memory polymers: experiments, theory, and numerical simulations. J. Mech. Phys. Solids 58, 1100–1124.

Sun, J.Y., Zhao, X., Illeperuma, W.R., Chaudhuri, O., Oh, K.H., Mooney, D.J., Vlassak, J.J., Suo, Z., 2012. Nature 489, 133–136.

Sun, T.L., Kurokawa, T., Kuroda, S., Ihsan, A.B., Akasaki, I., Sato, K., Haque, M.A., Nakajima, T., Gong, J.P., 2013. Nat. Mater. 12, 932–937.

Qi, H.J., Boyce, M.C., 2004. Constitutive model for stretch-induced softening of the stress-stretch behavior of elastomeric materials. J. Mech. Phys. Solids 52, 2187–2205.

Wang, X., Hong, W., 2012. A visco-poroelastic theory for polymeric gels. Proc. R. Soc. A 468, 3824.

Zhang, T., Lin, S., Yuk, H., Zhao, X., 2015. Predicting fracture energies and crack-tip fields of soft tough Materials. Extrem. Mech. Lett. 4, 1.

Zhao, X., 2012. A theory for large deformation and damage of interpenetrating polymer networks. J. Mech. Phys. Solids 60, 319.

Zhao, X., 2014. Multi-scale multi-mechanism design of tough hydrogels: building dissipation into stretchy networks. Soft Matter 10, 672.